Chem, Volume *7*

Supplemental information

Stereodynamics of *E*/*Z* isomerization in rotaxanes through mechanical shuttling and covalent bond rotation

Stefano Corra, Christiaan de Vet, Massimo Baroncini, Alberto Credi, and Serena Silvi

SUPPLEMENTAL INFORMATION

SUPPLEMENTAL EXPERIMENTAL PROCEDURES

1. Materials and methods

General materials. All reagents and chemicals were purchased from Sigma-Aldrich or VWR international and used as received unless otherwise stated. Flash column chromatography was performed using Sigma Aldrich Silica 40 (230-400 mesh size or 40-63 μm) as the stationary phase. Size exclusion chromatography was performed using Biorad Biobeads SX-1 as the stationary phase. Thin layer chromatography was performed on TLC Silica gel 60 F254 coated aluminum plates from Merck.

NMR Spectroscopy. NMR spectra were recorded on an Agilent DD2 spectrometer operating at 500 MHz. Chemical shifts are quoted in parts per million (ppm) relative to tetramethylsilane using the residual solvent peak as a reference standard and all coupling constants (*J*) are expressed in Hertz (Hz). For variable temperature experiments, the high temperatures were calibrated using a neat ethylene glycol sample. Line shape analysis of the NMR spectra was performed using iNMR. Data from magnetization transfer experiments were fitted using CIFIT to extract rates of the co-conformational equilibrium.

Mass spectrometry. High resolution mass spectrometry (HRMS) measurements were performed on a Waters Xevo G2-XS instrument equipped with an ESI source and a Q-TOF ion analyzer.

2. Synthetic procedures

2.1 Synthesis of $1^{2+}\cdot 2PF_6^-$ and $2^{2+}\cdot 2PF_6^-$

Compound **1b**$H^{3+}\cdot 3PF_6^-$ was synthesized according to a previously published procedure.[1] Analytical data are consistent with those previously reported.

For the NMR characterization of rotaxane stereoisomers superscript "*u*" and "*c*" were added to the assigned proton number to identify the protons laying on the uncomplexed and the complexed side of the axle respectively.

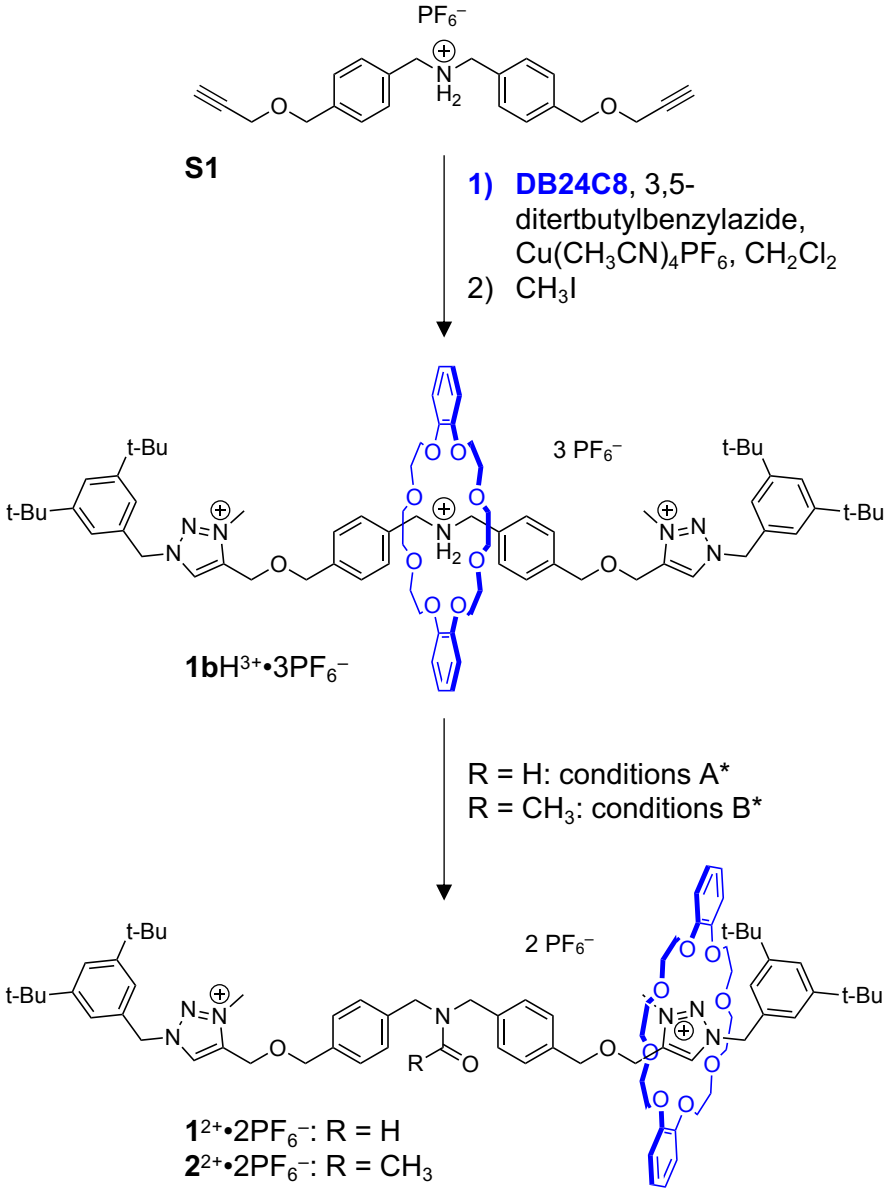

Scheme S1. Synthetic route towards compounds $\mathbf{1}^{2+}\cdot 2PF_6^-$ and $\mathbf{2}^{2+}\cdot 2PF_6^-$.
(*) *Conditions A:* 1) BEMP, 2) Ethyl formate, reflux. *Conditions B:* Ac_2O/CH_2Cl_2 1:1, r.t.

Formamide rotaxane $1^{2+}\cdot 2PF_6^-$

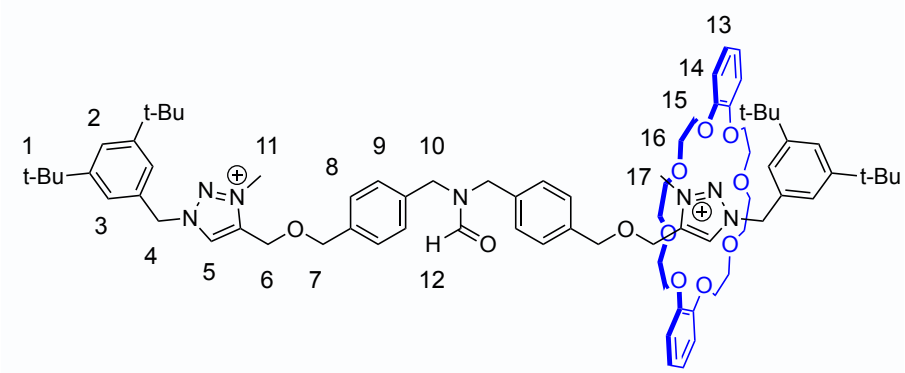

Rotaxane **1b**$H^{3+}\cdot 3PF_6^-$ (10 mg, 0.006 mmol) was dissolved in CH_2Cl_2, polymer bound 2-tertbutylimino-2-diethylamino-1,3-dimethylperhydro-1,3,2-diazaphosphorine (resin-bound BEMP) was added, and the suspension was shaken for 5 minutes. The resin was filtered, and the filtrate concentrated under reduced pressure. The residue was dissolved in ethyl formate (4 mL) and refluxed for 5 days under a nitrogen atmosphere. The solution was concentrated under reduced pressure and the residue was triturated with diethylether. The crude product was purified by size exclusion chromatography (Biobeads SX-1, CH_2Cl_2) to yield **1** as a pale yellow solid (8 mg, 0.005 mmol, 90%). **^{1}H-NMR (500 MHz, DMSO-d$_6$, 298 K):** *δ (ppm)* amide rotamer *Z*: 9.37 (s, 1H, H_5^c), 9.02 (s, 1H, H_5^u), 8.43 (s, 1H, H_{12}), 7.47 (s, 1H, H_2^c), 7.45 (s, 1H, H_2^u), 7.40 (s, 2H, H_3^c), 7.38 (d, *J* = 8.0 Hz, 2H, H_9^u), 7.36 (s, 2H, H_3^u), 7.23 (d, *J* = 7.8 Hz, 2H, H_8^u), 7.11-6.98 (m, 4H, H_9^c/H_8^c), 6.95 – 6.89 (m, 4H, H_{14}), 6.90 – 6.84 (m, 4H, H_{13}), 5.83 (s, 2H, H_4^c), 5.81 (s, 2H, H_4^u), 4.82 (s, 2H, H_6^u), 4.74 (s, 2H, H_6^c), 4.59 (s, 2H, H_7^u), 4.33-4.27 (m, 4H, H_7^c/H_{10}^u), 4.23 (s, 3H, H_{11}^u), 4.21 (s, 2H, H_{10}^c), 4.09 (s, 3H, H_{11}^c), 4.06-3.93 (m, 8H, H_{15}), 3.55 (dd, *J* = 11.6, 5.4 Hz, 4H, H_{16}), 3.51-3.42 (m, 4H, H_{16}), 3.27 (t, *J* = 4.7 Hz, 4H, H_{17}), 3.15 (dd, *J* = 10.9, 6.0 Hz, 4H, H_{17}), 1.28 (s, 18H, H_1^u), 1.22 (s, 18H, H_1^c). amide rotamer *E*: 9.37 (s, 1H, H_5^c), 9.04 (s, 1H, H_5^u), 8.45 (s, 1H, H_{12}), 7.47 (s, 1H, H_2^c), 7.45 (s, 1H, H_2^u), 7.40 (s, 2H, H_3^c), 7.36 (s, 2H, H_3^u), 7.34 (d, *J* = 7.8 Hz, 2H, H_9^u), 7.17 (d, *J* = 7.7 Hz, 1H, H_8^u), 7.11-6.98 (m, 4H, H_9^c/H_8^c), 6.95-6.89 (m, 4H, H_{14}), 6.90-6.84 (m, 4H, H_{13}), 5.84 (s, 2H, H_4^c), 5.81 (s, 2H, H_4^u), 4.83 (s, 2H, H_6^u), 4.70 (s, 2H, H_6^c), 4.61 (s, 2H, H_7^u), 4.33-4.27 (m, 4H, H_7^c/H_{10}^u), 4.24 (s, 3H, H_{11}^u), 4.19 (s, 2H, H_{10}^c), 4.08 (s, 3H, H_{11}^c), 4.06-3.93 (m, 8H, H_{15}), 3.55 (dd, *J* = 11.6, 5.4 Hz, 4H, H_{16}), 3.51-3.42 (m, 4H, H_{16}), 3.27 (t, *J* = 4.7 Hz, 4H, H_{17}), 3.15 (dd, *J* = 10.9, 6.0 Hz, 4H, H_{17}), 1.28 (s, 18H, H_1^u), 1.22 (s, 18H, H_1^c). **^{13}C-NMR (125 MHz, DMSO-d$_6$, 298 K):** *δ (ppm)* mixture of *E* and *Z*: 163.2, 151.3, 147.3, 136.2, 132.0, 129.5, 128.3, 128.2, 127.8, 127.7, 127.6, 123.3, 123.0, 121.1, 120.8, 112.1, 70.4, 70.2, 69.3, 69.1, 68.7, 67.8, 56.7, 38.3, 37.4, 34.6, 34.5, 31.1, 31.0. **HRMS (ESI+)** *m/z* calculated for $C_{79}H_{107}N_7O_{11}^{2+}$ $[M]^{2+}$ 665.9092; found: 665.9092.

Acetamide rotaxane $2^{2+}\cdot 2PF_6^-$

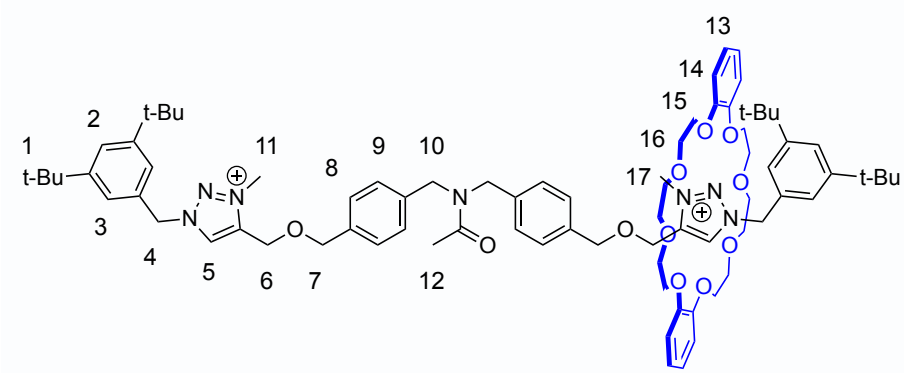

Rotaxane **1b**$H^{3+}\cdot 3PF_6^-$ (10 mg, 0.006 mmol) was dissolved in CH_2Cl_2/Ac_2O 1:1 (4 mL) under a nitrogen atmosphere and stirred overnight at room temperature. Volatiles were removed under reduced pressure. The residue was triturated with diethylether. The crude product was purified by size exclusion chromatography (Biobeads SX-1, CH_2Cl_2) to yield **2** as an off-white solid (9 mg, 0.005 mmol, 90%). **^{1}H-NMR (500 MHz, DMSO-d$_6$, 298 K):** *δ (ppm)* amide rotamer *Z*: 9.38 (s, 1H, H_5^c), 9.02 (s, 1H, H_5^u), 7.47 (s, 1H, H_2^c), 7.45 (s, 1H, H_2^u), 7.41 (s, 2H, H_3^c), 7.38 (d, *J* = 7.8 Hz, 2H, H_9^u), 7.36 (s, 2H, H_3^u), 7.21 (d, *J* = 7.8, 2H, H_8^u), 7.11-6.97 (m, 4H, H_8^c/H_9^c), 6.93 (dd, *J* = 6.0, 3.8 Hz, 4H, H_{13}), 6.87 (dd, *J* = 6.0, 3.6 Hz, 4H, H_{14}), 5.83 (s, 2H, H_4^c), 5.81 (s, 2H, H_4^u), 4.82 (s, 2H, H_6^u), 4.73 (s, 2H, H_6^c), 4.58 (s, 2H, H_7^u), 4.49-4.38 (m, 4H, H_7^c/H_{10}^u), 4.32 (s, 2H, H_{10}^c), 4.23 (s, 3H, H_{11}^u), 4.09 (s, 3H, H_{11}^c), 4.05-3.91 (m, 8H, H_{15}), 3.55 (dd, *J* = 11.5, 5.4 Hz, 4H, H_{16}), 3.47 (dd, *J* = 11.6, 6.1 Hz, 4H, H_{16}), 3.29-3.23 (m, 4H, H_{17}), 3.15 (dd, *J* = 10.9, 6.2 Hz, 4H, H_{17}), 2.08 (s, 3H, H_{12}), 1.28 (s, 18H, H_1^u), 1.22 (s, 18H, H_1^c). Amide rotamer *E*: 9.36 (s, 1H, H_5^c), 9.04 (s, 1H, H_5^u), 7.45 (s, 1H, H_2^u), 7.36 (s, 2H, H_3^u), 7.32 (d, *J* = 7.8 Hz, 2H, H_9^u), 7.20 (d, *J* = 7.9, 2H, H_8^u), 7.11-6.97 (m, 4H, H_9^c/H_8^c), 6.93 (dd, *J* = 6.0, 3.8 Hz, 4H, H_{13}), 6.87 (dd, *J* = 6.0, 3.6 Hz, 4H, H_{14}), 5.84 (s, 2H, H_4^c), 5.81 (s, 2H, H_4^u), 4.83 (s, 2H, H_6^u), 4.68 (s, 2H, H_6^c), 4.60 (s, 2H, H_7^u), 4.49-4.38 (m, 4H, H_7^c/H_{10}^u), 4.30 (s, 2H, H_{10}^c), 4.24 (s, 3H, H_{11}^u), 4.07 (s, 3H, H_{11}^c), 4.05-3.91 (m, 8H, H_{15}), 3.55 (dd, *J* = 11.5, 5.4 Hz, 4H, H_{16}), 3.47 (dd, *J* = 11.6, 6.1 Hz, 4H, H_{16}), 3.29-3.23 (m, 4H, H_{17}), 3.15 (dd, *J* = 10.9, 6.2 Hz, 4H, H_{17}), 2.07 (s, 3H, H_{12}), 1.28 (s, 18H, H_1^u), 1.22 (s, 18H, H_1^c). **^{13}C-NMR (125 MHz, DMSO-d$_6$, 298 K):** *δ (ppm)* mixture of *E* and *Z*: 170.3, 151.3, 150.8, 148.5, 147.4, 140.7, 137.5, 136.9, 132.0, 131.6, 129.5, 128.5, 128.2, 127.9, 127.7, 127.6, 127.4, 126.6, 126.3, 125.0, 123.3, 123.0, 121.2, 120.8, 112.2, 72.1, 72.0, 70.4, 70.2, 69.3, 69.2, 68.7, 67.8, 59.5, 56.8, 34.7, 34.6, 31.2, 31.1, 21.5. **HRMS (ESI+)** *m/z* calculated for $C_{80}H_{109}N_7O_{11}^{2+}$ $[M]^{2+}$ 672.9171; found: 672.9171.

2.2 Synthesis of free threads $1a^{2+}\cdot 2PF_6^-$ and $2a^{2+}\cdot 2PF_6^-$

Compound **S3** and 3,5-ditertbutylbenzyl azide were synthesized according to previously published procedures.[1,2]

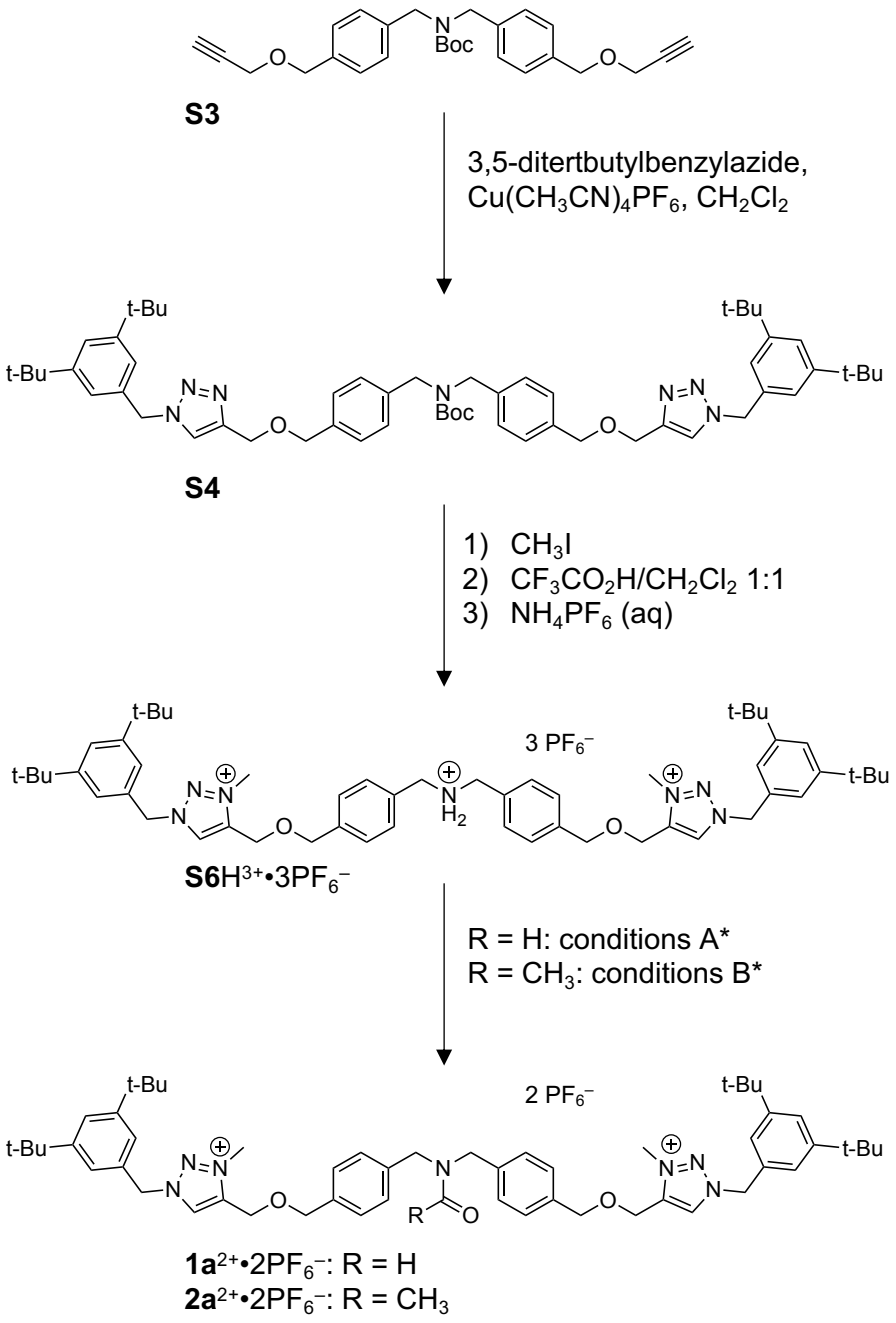

Scheme S2. Synthetic route towards compounds $\mathbf{1a}^{2+}\cdot 2PF_6^-$ and $\mathbf{2a}^{2+}\cdot 2PF_6^-$.
(*) *Conditions A:* 1) BEMP, 2) Ethyl formate, reflux. *Conditions B:* Ac_2O/CH_2Cl_2 1:1, r.t.

S4

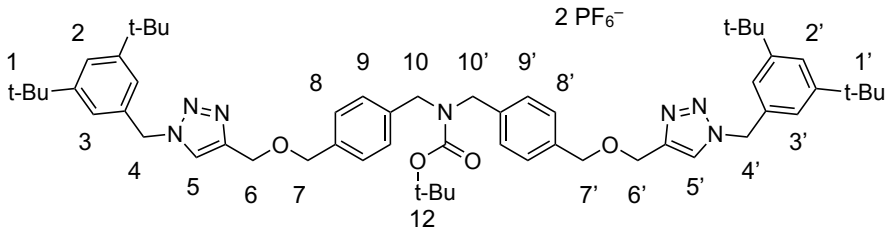

S3 (362 mg, 0.84 mmol), 3,5-di-(tertbutyl) benzyl azide (592 mg, 2.06 mmol), and $Cu(CH_3CN)_4PF_6$ (156 mg, 0.42 mmol) were dissolved in degassed CH_2Cl_2 (20 mL) and stirred overnight. The mixture was diluted with CH_2Cl_2, washed with an aqueous solution of EDTA (0.1 M), and water. The organic layer was dried over Na_2SO_4 and concentrated under vacuum. The crude product was purified by size exclusion chromatography (Biobeads SX-3, $CHCl_3$) to yield **S4** as a colorless glassy solid (372 mg, 0.40 mmol, 48%). **^{1}H NMR (500 MHz, $CDCl_3$, 298 K)** *δ (ppm)* 7.48 (s, 2H, $H_5/H_{5'}$), 7.41 (t, *J* = 1.8 Hz, 2H, $H_2/H_{2'}$), 7.28 (d, *J* = 7.8 Hz, 4H, $H_8/H_{8'}$), 7.22–7.13 (m, 4H, $H_9/H_{9'}$), 7.12 (d, *J* = 1.7 Hz, 6H, $H_3/H_{3'}$), 5.50 (s, 4H, $H_4/H_{4'}$), 4.67 (s, 4H, $H_6/H_{6'}$), 4.56 (s, 4H, $H_7/H_{7'}$), 4.37 (s, 2H, H_{10}), 4.28 (s, 2H, $H_{10'}$), 1.48 (s, 9H, H_{12}), 1.30 (s, 36H, $H_1/H_{1'}$). **^{13}C-NMR (125 MHz, $CDCl_3$, 298 K):** *δ (ppm)* 156.1, 151.9, 145.5, 136.9, 133.8, 128.3, 123.0, 122.6, 122.5, 80.2, 72.3, 63.9, 55.0, 35.0, 31.5, 28.3.

S5

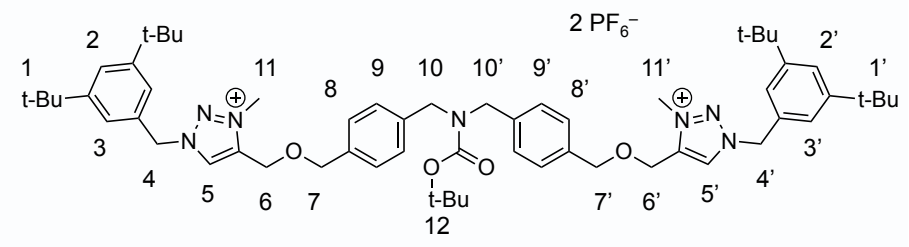

S4 (200 mg, 0.22 mmol) was dissolved in CH_3I (5 mL) and stirred at room temperature for four days under a nitrogen atmosphere. The solution was concentrated under reduced pressure, the residue was dissolved in the minimum amount of CH_2Cl_2 and dispersed in diethylether (200 mL). The suspension was centrifuged at 3000 rpm for 5 min, the supernatant was removed and the solid dispersed in fresh Et_2O. The procedure was repeated three times to afford **S5** as an off-white solid (150 mg, 0.12 mmol, 56%). **^{1}H NMR (500 MHz, $CDCl_3$, 298 K)** *δ (ppm)* 9.28 (s, 1H, H_5), 9.25 (s, 1H, $H_{5'}$), 7.48 (t, J = 1.8 Hz, 2H, $H_2/H_{2'}$), 7.40 (d, *J* = 1.8 Hz, 4H, $H_3/H_{3'}$), 7.24 (d, *J* = 7.7 Hz, 4H, $H_8/H_{8'}$), 7.19–7.04 (m, 4H, $H_9/H_{9'}$), 5.85 (s, 4H, $H_4/H_{4'}$), 4.91 (s, 2H, H_6), 4.89 (s, 2H, $H_{6'}$), 4.65 (s, 4H, $H_7/H_{7'}$), 4.42 (s, 4H, $H_{10}/H_{10'}$), 4.35 (s, 6H, $H_{11}/H_{11'}$), 1.49 (s, 9H, H_{12}), 1.32 (s, 36H, $H_1/H_{1'}$). **^{13}C-NMR (125 MHz, DMSO-d_6, 298 K):** *δ (ppm)* 155.9, 152.5, 140.4, 138.4, 135.1, 130.3, 130.2, 128.7, 128.4, 128.0, 124.3, 124.0, 80.3, 73.5, 59.9, 58.4, 31.5, 28.5.

S6

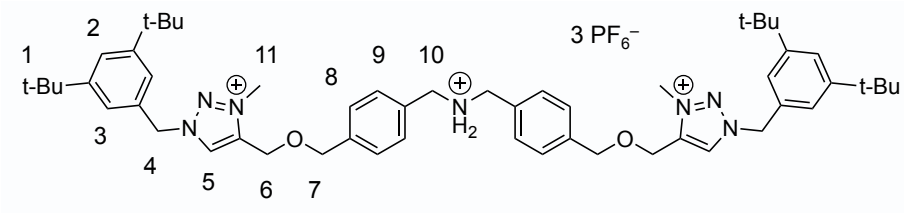

S5 (150 mg, 0.12 mmol) was dissolved in CF_3CO_2H/CH_2Cl_2 (1:1 v/v, 6 mL). After 2 h the solution was diluted with CH_2Cl_2 (90 mL) and washed with aqueous NaOH (1M, 2 x 50 mL). The organic layer was dried over Na_2SO_4 and concentrated under vacuum. The residue was dissolved in CH_2Cl_2 (15 mL), cooled to 0 °C, and gaseous HCl was bubbled through the solution for 10 min. The vessel was opened to air for 30 min to release the excess of HCl. The mixture was then diluted with acetone (7.5 mL) and stirred overnight after addition of an aqueous solution of NH_4PF_6 (sat., 15 mL). The organic layer was separated and washed with H_2O (2 x 10 mL), dried over Na_2SO_4, and concentrated to afford **S6** as an off-white solid (100 mg, 0.04 mmol, 35 %). **^{1}H NMR (500 MHz, CD_2Cl_2, 298 K)*** *δ (ppm)* 8.17 (s, 2H, H_5), 7.53 (t, *J* = 1.6 Hz, 2H, H_2), 7.36 (d, *J* = 7.9 Hz, 4H, H_8), 7.32–7.20 (m, 8H, H_3/H_9), 5.63 (s, 4H, H_4), 4.68 (s, 4H, H_6), 4.61 (s, 4H, H_7), 4.23 (s, 6H, H_{11}), 3.79 (s, 4H, H_{10}), 1.32 (s, 36H, H_1). **^{13}C-NMR (125 MHz, CD_2Cl_2, 298 K)*** *δ (ppm)* 153.2, 141.4, 135.4, 130.2, 129.3, 129.2, 129.0, 125.1, 124.4, 74.1, 59.5, 59.1, 53.0, 39.1, 35.4, 31.6.

(*) The compound was deprotonated *in situ* with polymer-bound BEMP prior to characterization to facilitate comparison of the spectra with those of the final compounds.

$1a^{2+}\cdot 2PF_6^-$

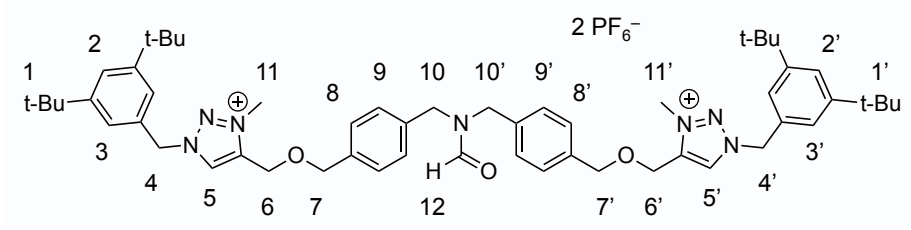

S6 (11 mg, 0.009 mmol) was dissolved in CH_2Cl_2, polymer-bound BEMP base was added and the suspension shaken for 5 minutes. The resin was filtered, and the filtrate concentrated under reduced pressure. The residue was dissolved in ethyl formate (4 mL) and refluxed for 5 days under a nitrogen atmosphere. The solution was concentrated under reduced pressure. The residue was triturated with diethylether and dried under high vacuum to yield **$1a^{2+}$** as a pale yellow solid (10 mg, 0.009 mmol, 95%). **^{1}H-NMR (500 MHz, DMSO-d_6, 298 K):** *δ (ppm)* 9.03 (s, 1H, H_5), 9.02 (s, 1H, $H_{5'}$), 8.46 (s, 1H, H_{12}), 7.45 (s, 2H, $H_2/H_{2'}$), 7.37 (d, *J* = 7.9 Hz, 2H, H_8), 7.36 (dd, *J* = 1.7, 0.8 Hz, 4H, $H_3/H_{3'}$), 7.33 (d, *J* = 8.0 Hz, 2H, $H_{8'}$), 7.24 (d, *J* = 7.9 Hz, 2H, H_9), 7.18 (d, *J* = 7.8 Hz, 2H, $H_{9'}$), 5.81 (s, 2H, H_4), 5.80 (s, 2H, $H_{4'}$), 4.83 (s, 2H, H_6), 4.82 (s, 2H, $H_{6'}$), 4.60 (s, 2H, H_7), 4.59 (s, 2H, $H_{7'}$), 4.34 (s, 2H, H_{10}), 4.25 (s, 2H, $H_{10'}$), 4.24 (s, 3H, H_{11}), 4.23 (s, 3H, $H_{11'}$), 1.28 (s, 36H, $H_1/H_{1'}$). **^{13}C-NMR (125 MHz, DMSO-d_6, 298 K):** *δ (ppm)* 163.8, 151.8, 140.9, 140.8, 137.0, 136.5, 132.2, 129.7, 129.6, 128.7, 128.6, 128.3, 128.1, 123.6, 123.4, 72.4, 72.3, 63.9, 59.8, 57.2, 49.8, 44.2, 38.5, 34.9, 31.5

$2a^{2+}\cdot 2PF_6^-$

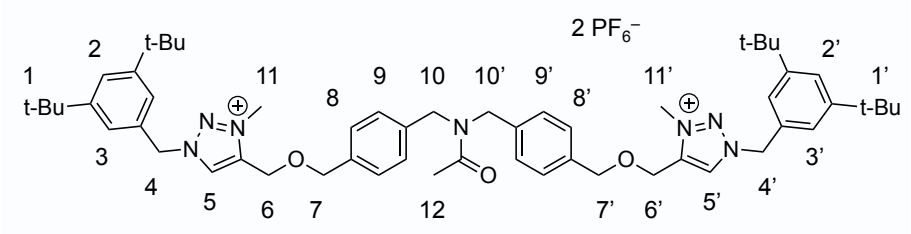

S6 (10 mg, 0.008 mmol) was dissolved in CH_2Cl_2/Ac_2O 1:1 (4 mL) under a nitrogen atmosphere and stirred overnight at room temperature. Volatiles were removed under reduced pressure. The residue was triturated with diethylether and dried under high vacuum to yield **$2a^{2+}$** as an off-white solid (9 mg, 0.007 mmol, 95%). **^{1}H-NMR (500 MHz, DMSO-d_6, 298 K):** *δ (ppm)* 9.03 (s, 1H, H_5), 9.01 (s, 1H, $H_{5'}$), 7.44 (s, 2H, $H_2/H_{2'}$), 7.38-7.31 (m, 8H, $H_3/H_{3'}/H_8/H_9$), 7.22-7.19 (m, 4H, $H_{8'}/H_{9'}$), 5.80 (s, 4H, $H_4/H_{4'}$), 4.82 (s, 2H, H_6), 4.81 (s, 2H, $H_{6'}$), 4.59 (s, 2H, H_7), 4.58 (s, 2H, $H_{7'}$), 4.49 (s, 2H, H_{10}), 4.45 (s, 2H, $H_{10'}$), 4.23 (s, 6H, $H_{11}/H_{11'}$), 2.08 (s, 3H, H_{12}), 1.27 (s, 36H, $H_1/H_{1'}$). **^{13}C-NMR (125 MHz, DMSO-d_6, 298 K):** *δ (ppm)* 170.3, 151.3, 140.6, 137.5, 137.1, 136.2, 135.9, 132.0, 129.4, 128.4, 128.2, 127.6, 126.6, 123.3, 123.0, 72.0, 71.9, 59.6, 59.5, 56.7, 50.5, 47.6, 38.2, 34.6, 31.1, 21.4

3. Dynamic NMR experiments

3.1. Determination of the absolute stereochemistry of rotamers of $\mathbf{1}^{2+}\cdot 2PF_6^-$

^{1}H-^{1}H NOESY was exploited to assign the absolute stereochemistry of the rotamers of $\mathbf{1}^{2+}\cdot 2PF_6^-$. To the axle side encircled by the ring is given a higher priority in the assignment.[3] NOE signals between H_{12} and $H_{10}^{u/Z}$ or $H_{10}^{c/E}$ are diagnostic of the *Z* and *E* amide stereoisomers, respectively. Moreover, exchange cross-peaks are consistent with the assignment of H_{10} for the two rotamers.

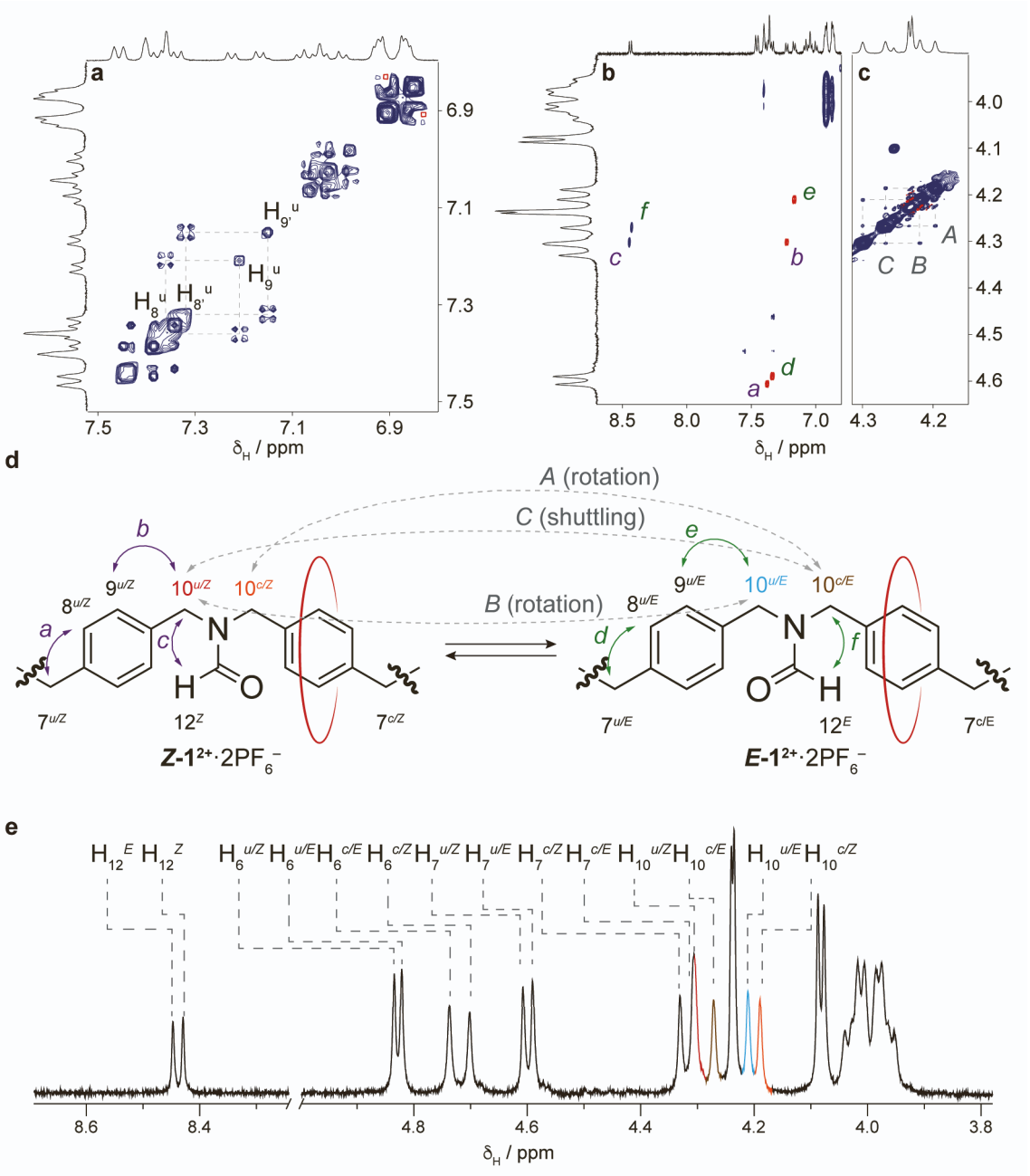

Figure S1. Dynamic NMR experiments on rotaxane $\mathbf{1}^{2+}$. a) Partial TOCSY spectrum (500 MHz, DMSO-d_6, 298 K, spinlock 80 ms) in the region of aromatic protons. b) Partial NOESY spectrum (500 MHz, DMSO-d_6, 298 K, t_{mix} = 0.4 s) in the region of aromatic-aliphatic NOEs. c) Partial EXSY spectrum (500 MHz, DMSO-d_6, 318 K, t_{mix} = 0.4 s) in the region of aliphatic signals. d) Chemical exchange between non-equivalent protons (capital letters, gray dashed arrows) and NOE mapping (small letters, solid arrows) for *Z*-$\mathbf{1}^{2+}$ (purple) and for *E*-$\mathbf{1}^{2+}$ (green). The red ring indicates the side of the axle where the DB24C8 macrocycle is located. NOEs "*c*" (H_{12}^{Z}-$H_{10}^{u/Z}$) and "*f*" (H_{12}^{E}-$H_{10}^{c/E}$) are indicative of the *Z* and *E* stereoisomers of $\mathbf{1}^{2+}$. e) Partial ^{1}H NMR spectrum (500 MHz, DMSO-d_6, 298 K) of $\mathbf{1}^{2+}$ with assignments for the *E* and *Z* rotamers. Signals for H_{10} set are color-coded according to the reaction scheme above.

3.2. Variable temperature ^{1}H NMR

To elucidate the dynamics of the systems ^{1}H NMR spectra of $\mathbf{1}^{2+}\cdot 2PF_6^-$, $\mathbf{1a}^{2+}\cdot 2PF_6^-$,$\mathbf{2}^{2+}\cdot 2PF_6^-$, and $\mathbf{2a}^{2+}\cdot 2PF_6^-$ were recorded in DMSO-d_6 between 298 K and 398 K and in $CDCl_3$ between 298 K and 338 K at 10 K intervals. ^{1}H NMR spectra of $\mathbf{1b}^{2+}\cdot 2PF_6^-$ were recorded in $CDCl_3$ between 243 K and 303 K and in DMSO-d_6 between 298 K and 328 K. The rates of exchange as a function of temperature were determined from visual comparisons of experimental spectra with line shapes computed using iNMR, or, in the case of $\mathbf{1b}^{2+}\cdot 2PF_6^-$ in DMSO-d_6, estimated from the residual line broadening after coalescence.

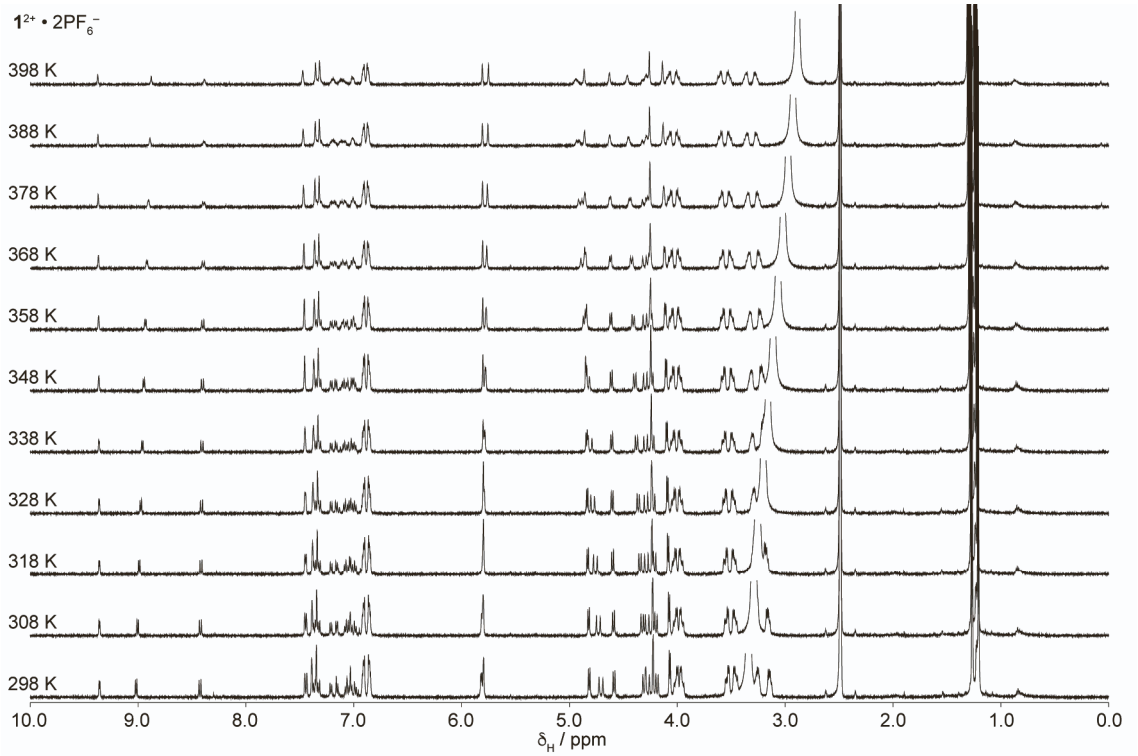

Figure S2. Variable temperature ^{1}H-NMR spectra of $\mathbf{1}^{2+}\cdot 2PF_6^-$ (500 MHz, DMSO-d_6).

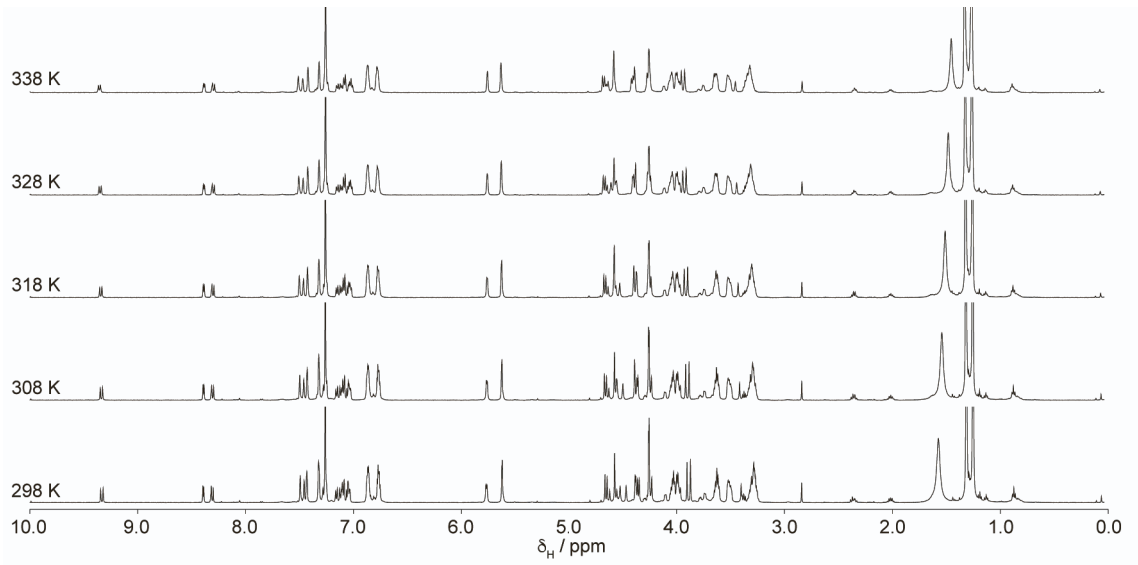

Figure S3. Variable temperature ^{1}H-NMR spectra of $\mathbf{1}^{2+}\cdot 2PF_6^-$ (500 MHz, $CDCl_3$).

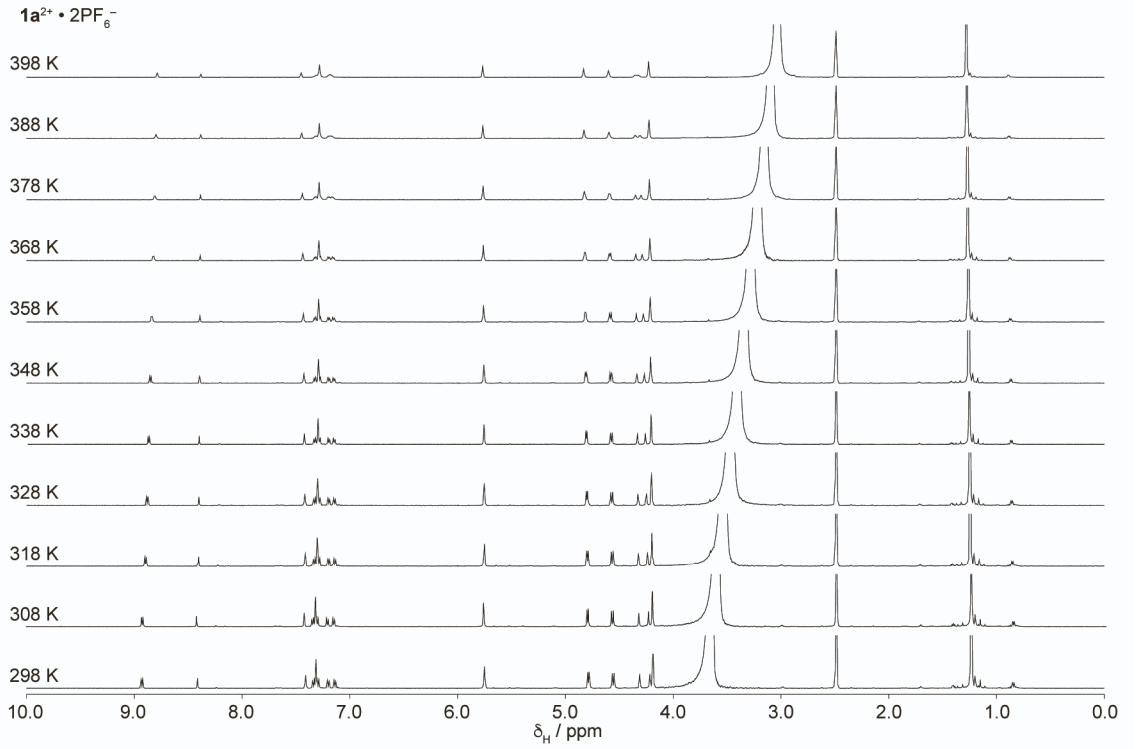

Figure S4. Variable temperature ^{1}H-NMR spectra of **1a**$^{2+}$·2PF_6^- (500 MHz, DMSO-d_6).

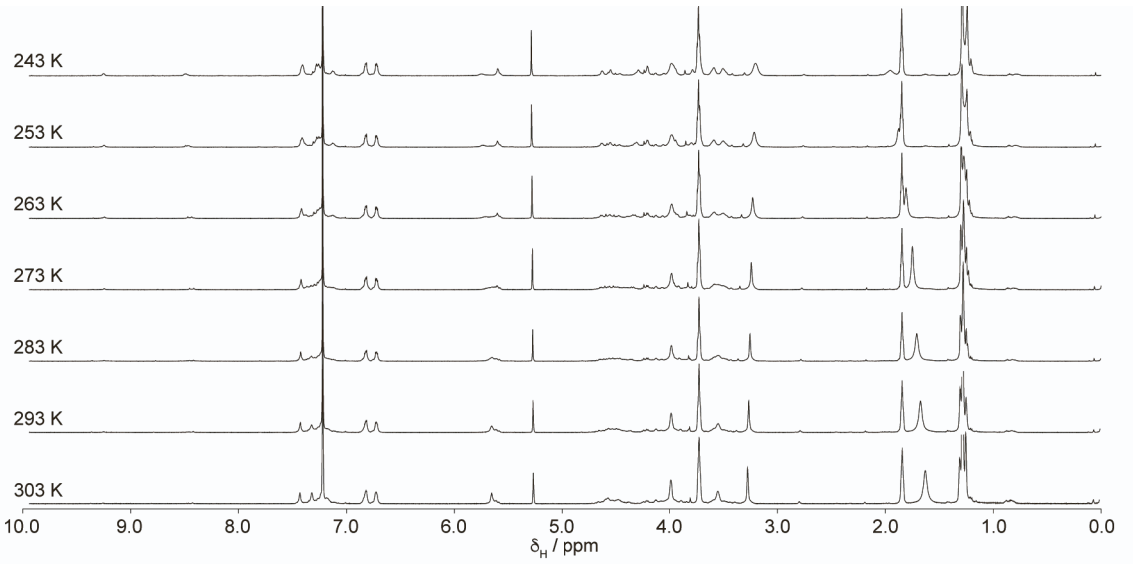

Figure S5. Variable temperature ^{1}H-NMR spectra of **1b**$^{2+}$·2PF_6^- (500 MHz, $CDCl_3$).

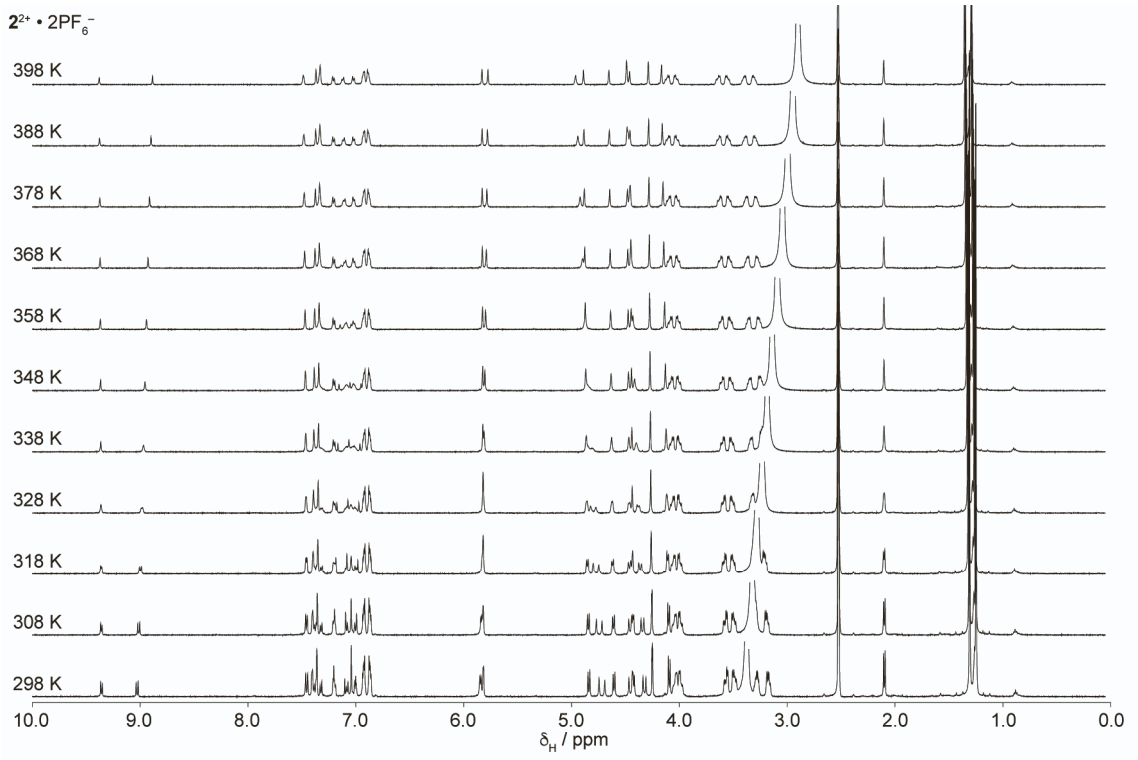

Figure S6. Variable temperature ^{1}H-NMR spectra of $\mathbf{2}^{2+} \cdot 2PF_6^-$ (500 MHz, DMSO-d_6).

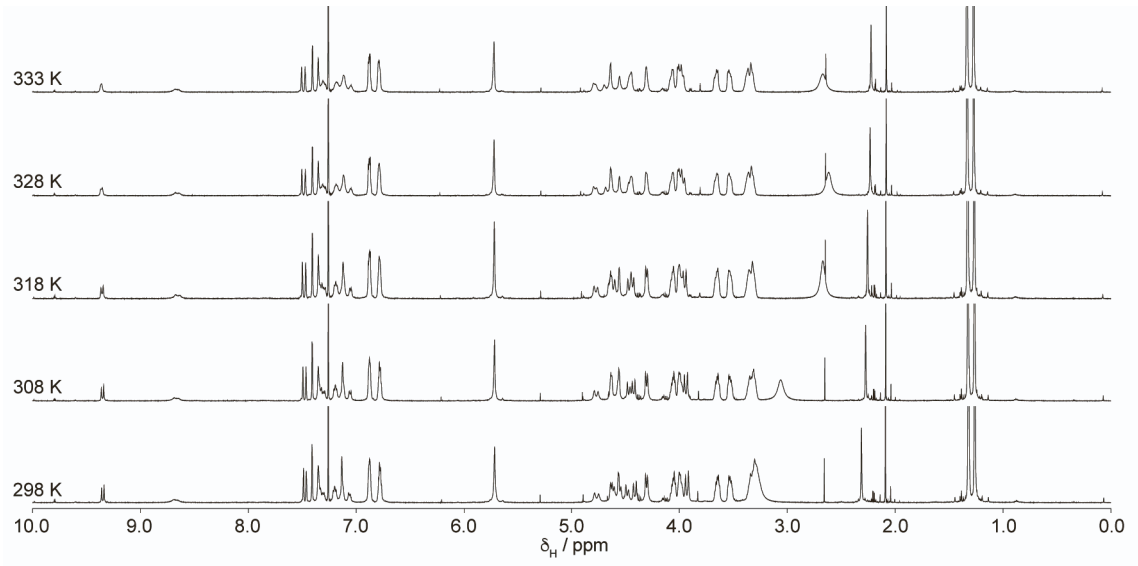

Figure S7. Variable temperature ^{1}H-NMR spectra of $\mathbf{2}^{2+} \cdot 2PF_6^-$ (500 MHz, $CDCl_3$).

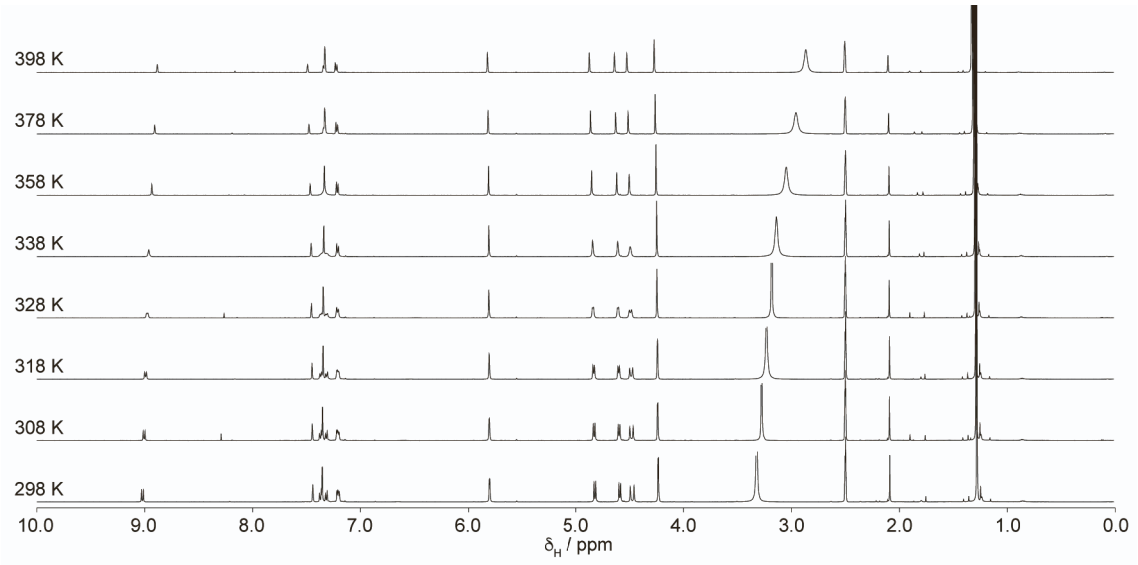

Figure S8. Variable temperature ^{1}H-NMR spectra of **2a**$^{2+}$·2PF$_6^-$ (500 MHz, DMSO-d$_6$).

Table S1. Experimental rate constants in the intermediate exchange regime on the ^{1}H NMR timescale for **1**$^{2+}$·2PF$_6^-$, **1a**$^{2+}$·2PF$_6^-$, **2**$^{2+}$·2PF$_6^-$, and **2a**$^{2+}$·2PF$_6^-$, in DMSO-d$_6$.

	Rate constants (s^{-1})				
T (K)	**1**$^{2+}$·2PF$_6^-$ (rotation)	**1**$^{2+}$·2PF$_6^-$ (shuttling)	**1a**$^{2+}$·2PF$_6^-$ (rotation)	**2**$^{2+}$·2PF$_6^-$ (rotation)	**2a**$^{2+}$·2PF$_6^-$ (rotation)
308	*(a)*	*(a)*	*(a)*	3.5	3.2
318	2.5*(b)*	0.04*(b)*	0.7*(b)*	7.1	6.7
328	3.5*(b)*	0.08*(b)*	1.2*(b)*	14.2	13.8
338	4.4*(b)*	0.12*(b)*	1.7*(b)*	29.2	22.8
348	5.1	0.15	1.9	*(c)*	*(c)*
358	6.2	0.2	2.9	*(c)*	*(c)*
368	9.2	0.3	5.3	*(c)*	*(c)*
378	12.8	0.5	9.7	*(c)*	*(c)*
398	20.6	1.1	21.5	*(c)*	*(c)*

(a) Too slow to be determined by line-shape analysis; *(b)* exchange rate constants excluded from the Eyring analysis; *(c)* value not determined.

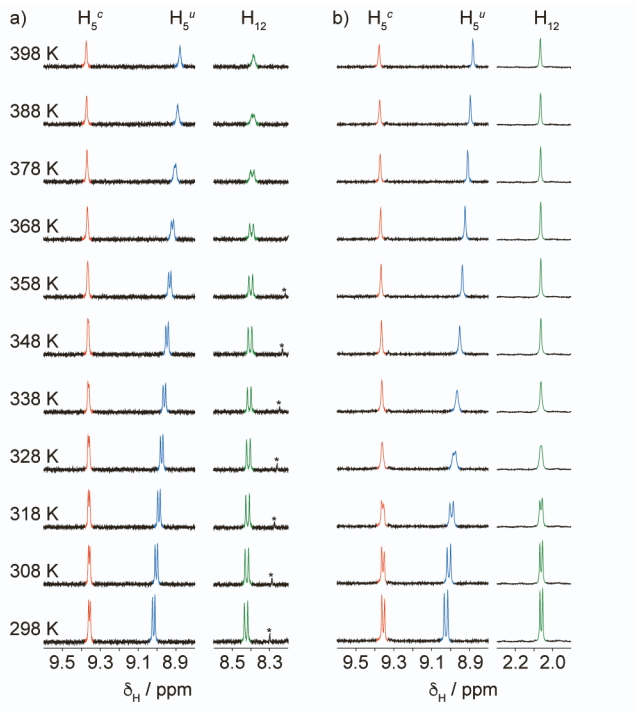

Figure S9. Partial ^{1}H-NMR (500 MHz, DMSO-d_6) spectra of $\mathbf{1}^{2+}\cdot 2PF_6^-$ (a), and $\mathbf{2}^{2+}\cdot 2\ PF_6^-$ (b) at different temperatures in the regions of the triazolium protons ($H_5^{c/E}$, $H_5^{c/Z}$, $H_5^{u/E}$, $H_5^{u/Z}$; left) and of the amide protons (H_{12}; right). For proton labeling refer to scheme 1 in the manuscript. The low-intensity signal marked with the star (*) belongs to an unidentified impurity.

The upfield shift of resonance H_{12} observed for $\mathbf{1}^{2+}$ with increasing temperature can be ascribed to a weak CH-π interaction between H_{12} and the DB24C8 ring.[4] Such a drift is not observed in rotaxane $\mathbf{2}^{2+}$ where proton H_{12} is replaced by a methyl group.

3.3 Selective Inversion Recovery ^{1}H NMR experiments in DMSO-d_6

To study the co-conformational isomerization process, magnetization transfer experiments were performed. A PRESAT (Agilent) pulse sequence was employed to selectively invert the H_5^c spin population (9.37 ppm). Calibration of the soft 180° pulse on $H_5^{c/E/Z}$ was achieved optimizing the pulse width (satdly).[5] Spectra were acquired at increasing mixing times (d2) ranging from 0 to 6 s. The co-conformational equilibrium of rotaxane $\mathbf{1}^{2+}$ converts $H_5^{c/E/Z}$ spins to $H_5^{u/E/Z}$, thus acquisition of spectra at different mixing times enables the extraction of spin-lattice relaxation times (T_1) and chemical exchange rate constants.

To ensure that H_5^c was present as a single set of spin, all experiments were performed above the coalescence temperature of H_5^c (348 K). To extract the activation parameters of the ring shuttling kinetics in rotaxane $\mathbf{1}^{2+}$, magnetization transfer experiments were performed at four different temperatures (353, 363, 373, and 383 K).

Peak intensity (magnetization) of protons H_5^u and H_5^c versus delay time (d2) were fitted using the CIFIT software to extract the chemical exchange rate constant.[6,7]

To increase the accuracy of the fitted parameters, the apparent spin-lattice relaxation time constants (T_1) of H_5^c and H_5^u were determined from an unselective relaxation experiment at 298 K. The exchange rate obtained using these initial T_1's was then used to extract improved T_1's and this iteration was continued until convergence of all parameters ($k_{shuttling}$ and T_1). Fit results and the corresponding best-fit parameters are reported in figure S10 and in table S3, respectively.

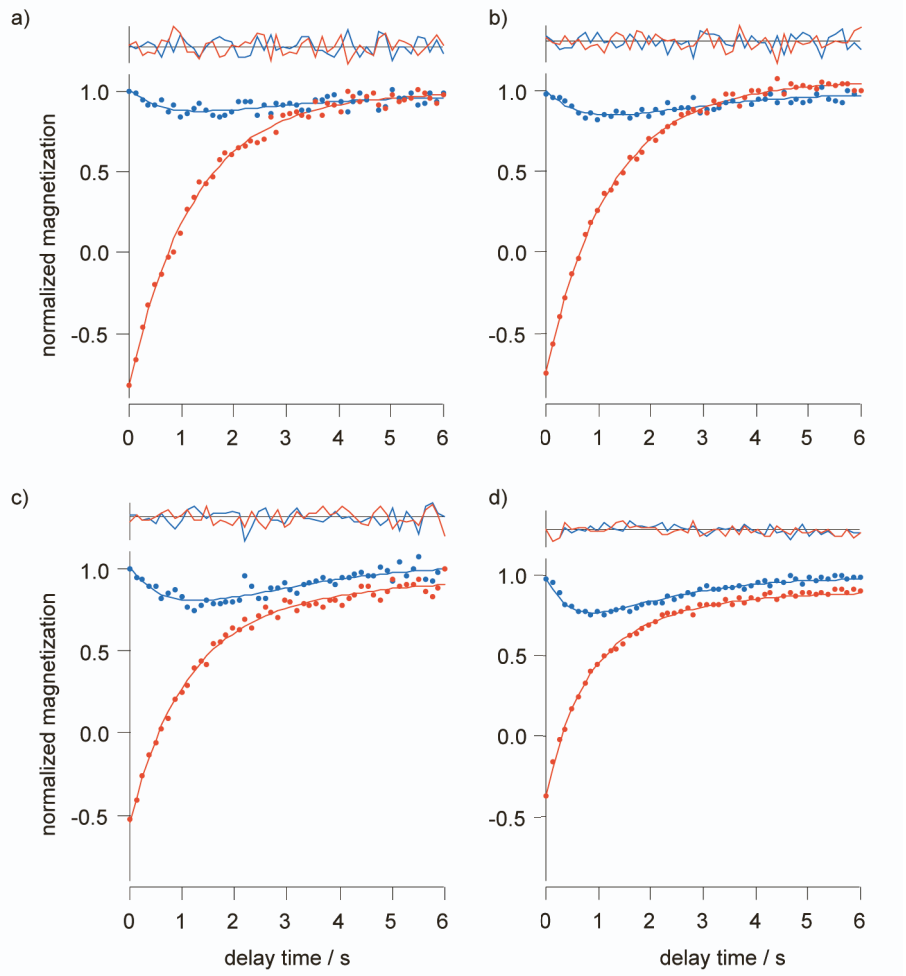

Figure S10. Comparison between the observed intensities (dots) of $H_5^{c/E/Z}$ (orange) and $H_5^{u/E/Z}$ (blue) in $\mathbf{1}^{2+}\cdot 2PF_6^-$ and those calculated from the best-fit parameters (solid lines) at different temperatures: 353 K (a), 363 K (b), 373 K (c), and 383 K (d). Fitting residuals are plotted above each graph.

Table S3. Rate constants of the co-conformational equilibrium, and spin-lattice relaxation time (T_1) for $H_5^{c/E/Z}$ and $H_5^{u/E/Z}$ extracted by fitting of the magnetization transfer data.

T (K)	$k_{shuttling}$ (s^{-1})	T_1 (s)	
		H_5^u	H_5^c
353	0.15	1.5	1.4
363	0.20	1.6	1.5
373	0.35	2.8	1.8
383	0.60	1.5	1.6

3.4 Exchange spectroscopy (EXSY) in DMSO-d_6

EXSY spectra of $\mathbf{1}^{2+}\cdot 2PF_6^-$ and $\mathbf{2}^{2+}\cdot 2PF_6^-$ in DMSO-d_6 were recorded at 363 K using a NOESY pulse sequence. Off-diagonal in-phase cross peaks between H_5^u and H_5^c signal sets observed for $\mathbf{1}^{2+}$ at t_{mix} > 0 s are indicative of chemical exchange ascribed to ring shuttling. The shuttling rate constant at 363 K determined using EXSYCalc is 0.14 s^{-1}. This result is fully consistent with that of the selective inversion recovery experiment at the same temperature.

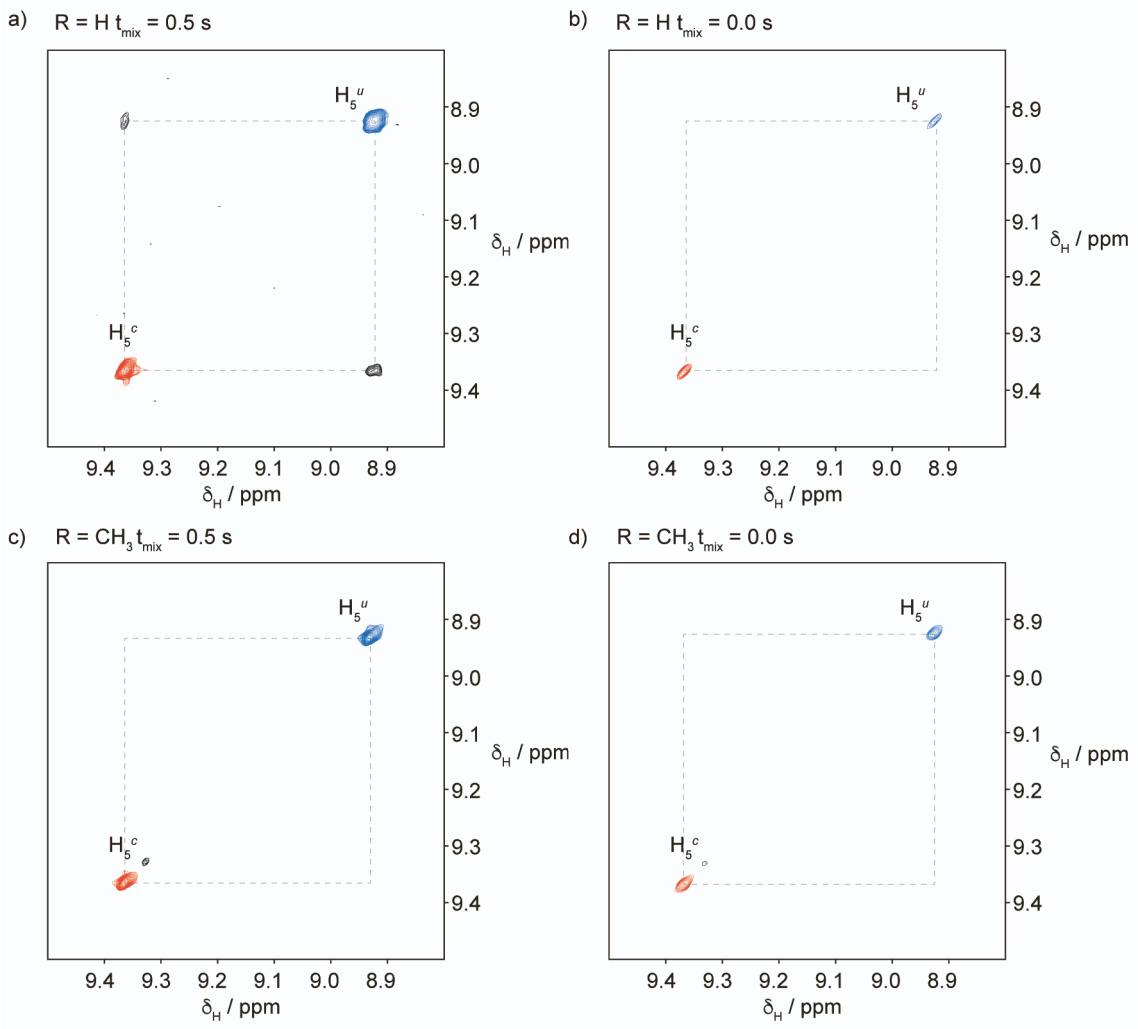

Figure S11. Partial EXSY spectra (500 MHz, 363 K) in the region of $H_5^{c/E/Z}$ (orange) and $H_5^{u/E/Z}$ (blue) of $\mathbf{1}^{2+}\cdot 2PF_6^-$ (a and b) and $\mathbf{2}^{2+}\cdot 2PF_6^-$ (c and d) at mixing times 0.5 s (a and c) and 0.0 s (b and d).

3.5 Estimation of the activation parameters of ring shuttling for $1b^{2+}$ in DMSO-d_6

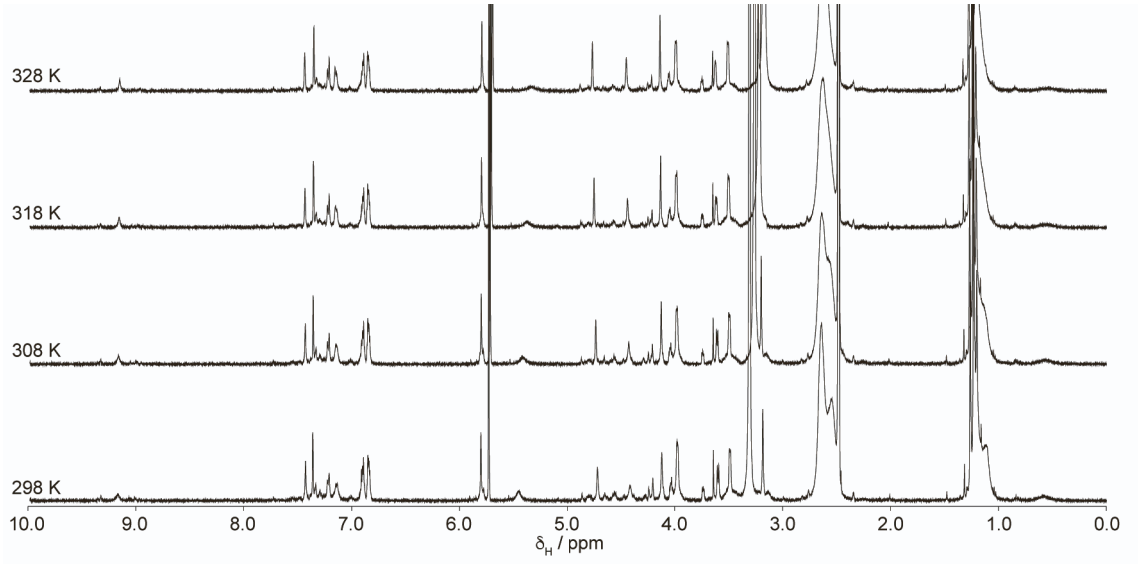

Figure S12. Variable temperature ^{1}H-NMR spectra of $\mathbf{1b}^{2+}\cdot 2PF_6^-$ (500 MHz, DMSO-d_6).

Deprotonation of rotaxane $\mathbf{1b}^{2+}$ in DMSO-d_6 using P1-base revealed that ring shuttling is fast in the NMR timescale. The coalescence temperature of resonances $H_5{}^c$ and $H_5{}^u$ is below 298 K. Nonetheless, a rough estimate of the activation parameters for the shuttling process in DMSO-d6 was obtained upon determination of the residual line broadening of resonances $H_5{}^c$ and $H_5{}^u$ after coalescence at different temperatures. The residual broadening and the rate constant are related by equation 1.

$$\mathrm{k} = \frac{\pi \Delta \upsilon_{AB}}{2\left(\Delta \upsilon_0 - \Delta \upsilon_{ref}\right)}$$

Equation 1. Eyring equation. $\Delta\nu_{AB}$: frequency difference of the two signals in slow exchange; $\Delta\nu_0$: line broadening of coalesced signals (FWHM); $\Delta\nu_{ref}$: FWHM of a non-exchanging peak (2.88 Hz).

FWHM were obtained by fitting the resonance with a Lorentzian function (Figure S15a, middle). Since it proved impossible to reach a temperature where signals $H_5{}^c$ and $H_5{}^u$ are in slow exchange due to the melting point of DMSO (18.5 °C), the frequency difference ($\Delta\nu_{AB}$) between the two signals was assumed to be 0.44 ppm. Such a value was based on what had been previously observed by Coutrot and coworkers which reported that difference in chemical shifts for an encircled and an unencircled triazolium in slow exchange in DMSO-d_6.[8] Rate constants at four different temperatures were, thus estimated using equation 1, and were used for Eyring analysis (Figure S15b).

Total lineshape analysis of the peaks by estimating a $\Delta\nu_{AB}$ of 0.44 ppm also provided comparable exchange rate constants to those obtained from eq. 1 (Figure S15a, right).

Table S2. FWHM extracted by fitting the resonance at 9.1 ppm. Exchange rate constants of the co-conformational equilibrium obtained from equation 2 and by total lineshape analysis.

T (K)	FWHM (Hz)	$k_{shuttling}$ (s^{-1})	
		LB	LSA
298	18.4	5024	5078
308	13.2	7539	7578
318	10.5	10154	9015
328	8.4	13978	11115

LB: residual line broadening; LSA: lineshape analysis.

3.6. Determination of the activation parameters in DMSO-d_6 and $CDCl_3$

The enthalpy ($\Delta H^{\ddagger}$) and entropy ($\Delta S^{\ddagger}$) of activation for amide rotation and ring shuttling were extrapolated by fitting the Eyring plots of corresponding exchange rate constants (k_{obs}) *vs* the reciprocal of absolute temperature (T) using equation 2.

$$\ln\left(\frac{k_{obs}}{T}\right) = -\frac{\Delta H^{\ddagger}}{RT} + \frac{\Delta S^{\ddagger}}{R} + \ln\frac{k_B}{h}$$

Equation 2. Eyring equation. R: ideal gas constant; h: Plank's constant; k_B: Boltzmann's constant.

3.6.1. Total lineshape analysis and Eyring plots in DMSO-d_6

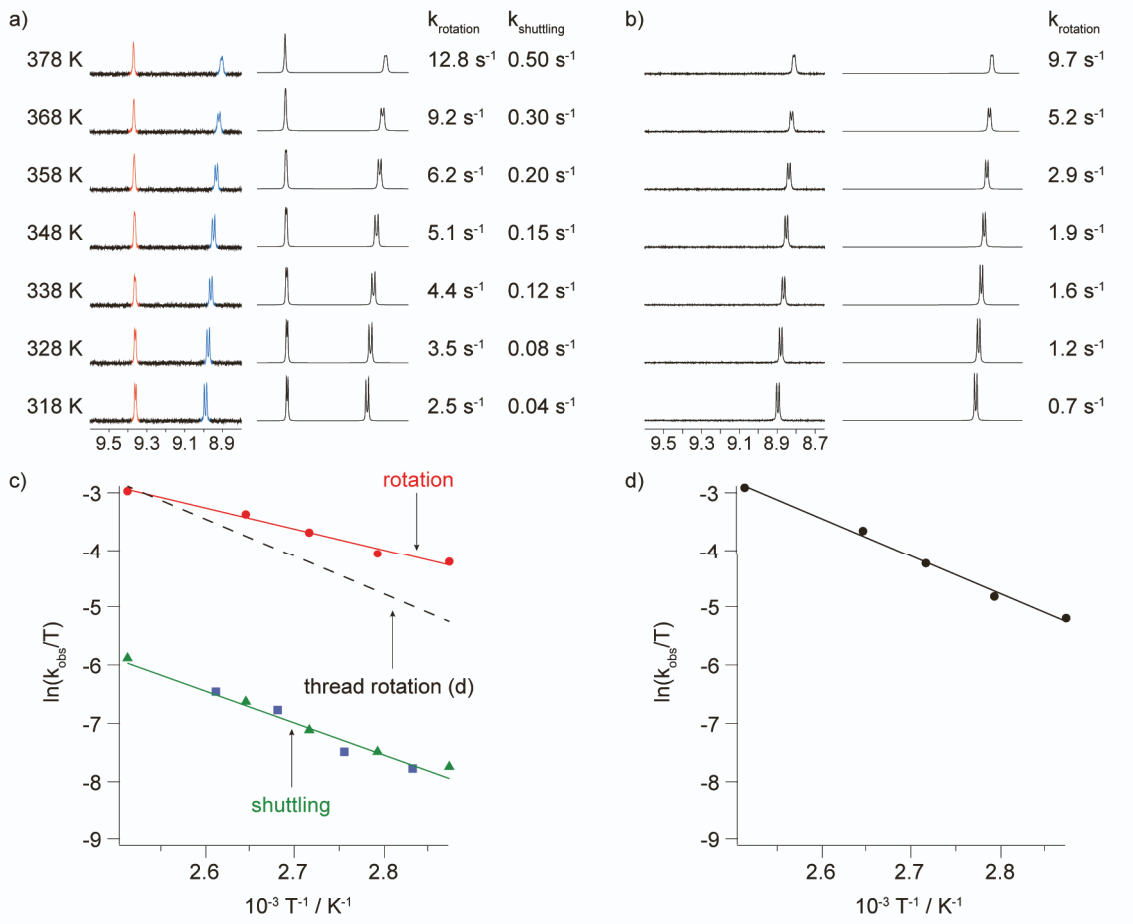

Figure S13. Partial ^{1}H-NMR (500 MHz, DMSO-d_6) spectra of **1**$^{2+}$·2PF_6^- (a) and **1a**$^{2+}$·2PF_6^- (b) at different temperatures (left) and corresponding simulated NMR spectra of the exchanging protons $H_5^{u/E}$, $H_5^{u/Z}$, $H_5^{c/E}$, and $H_5^{c/Z}$ (right). Sets of exchange rate constants ($k_{rotation}$, and $k_{shuttling}$) are reported on the right column (for assignment see text). c) Eyring plot for the rotation (red) and shuttling (green) processes in **1**$^{2+}$·2PF_6^-. Purple squares are exchange rate constants of shuttling univocally determined by magnetization transfer (see section 3.2). d) Eyring plot of the sole amide rotation process in **1a**$^{2+}$·2PF_6^-.

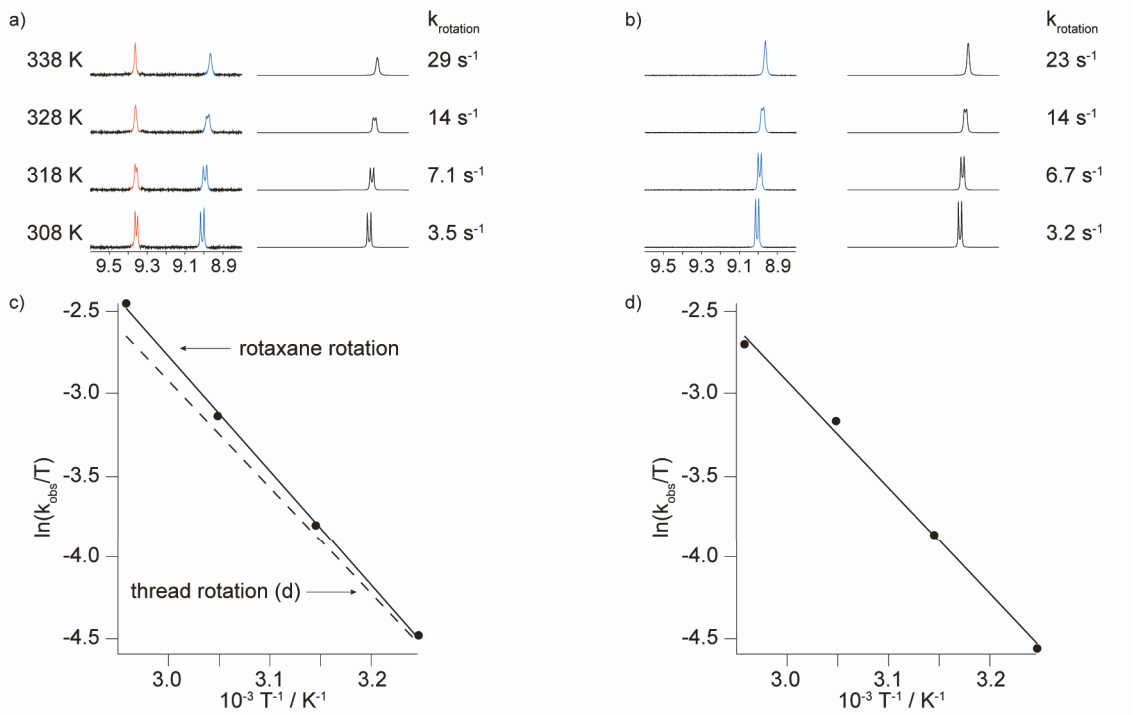

Figure S14. Partial ^{1}H-NMR (500 MHz, DMSO-d_6) spectra of $\mathbf{2}^{2+}\cdot 2PF_6^-$ (a) and $\mathbf{2a}^{2+}\cdot 2\ PF_6^-$ (b) at different temperatures (left) and corresponding simulated NMR spectra of the exchanging protons $H_5^{u/E}$ and $H_5^{u/Z}$ (right). Corresponding exchange rate constants ($k_{rotation}$) are reported on the right column (for assignment see text). c) Eyring plot for the rotation process in $\mathbf{2}^{2+}\cdot 2PF_6^-$. d) Eyring plot of the sole amide rotation process in $\mathbf{2a}^{2+}\cdot 2PF_6^-$.

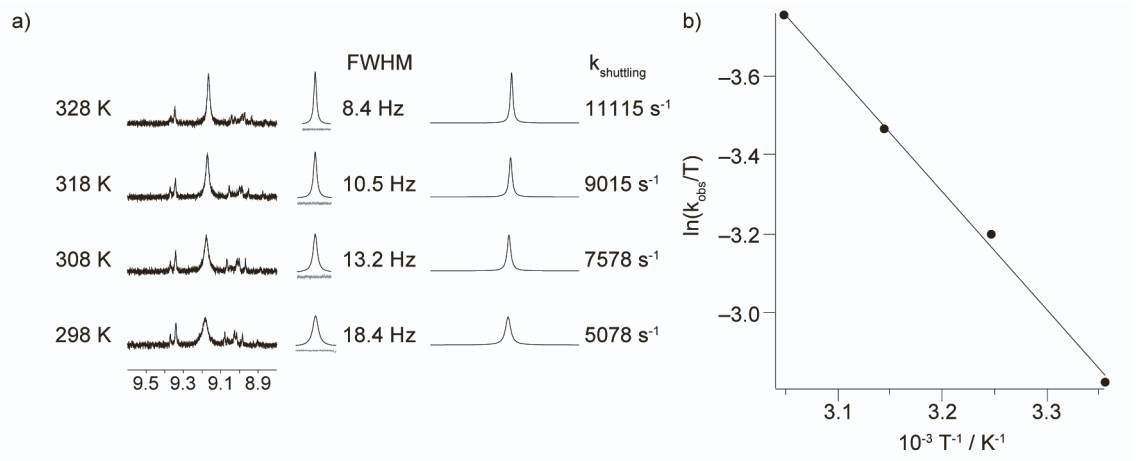

Figure S15. Partial ^{1}H-NMR (500 MHz, DMSO-d_6) spectra (a) of $\mathbf{1b}^{2+}\cdot 2PF_6^-$ at different temperatures (left), Lorentzian deconvolution (middle, residues are plotted in gray), and corresponding simulated NMR spectra for the exchanging protons H_5^{u} and H_5^{c} (right). b) Eyring plot for the shuttling process in $\mathbf{1b}^{2+}\cdot 2PF_6^-$.

3.6.2. Total lineshape analysis and Eyring plots in $CDCl_3$

Total lineshape analysis was performed in $CDCl_3$ for $\mathbf{1}^{2+}$, $\mathbf{2}^{2+}$, and $\mathbf{1b}^{2+}$. In the case of $\mathbf{1}^{2+}$, total lineshape analysis was performed on protons H_4, since the rotation process was too slow on the ^{1}H NMR timescale to observe appreciable variations in signals H_5. Moreover, contrarily to the experiments performed in DMSO-d_6, an adequate simulation of the spectra lineshapes could be obtained without considering a shuttling equilibrium. In fact, the shuttling mechanism was not detected by SIR experiments at temperatures compatible with the boiling point of the solvent ($T_{b,CDCl3}$ = 61 °C).

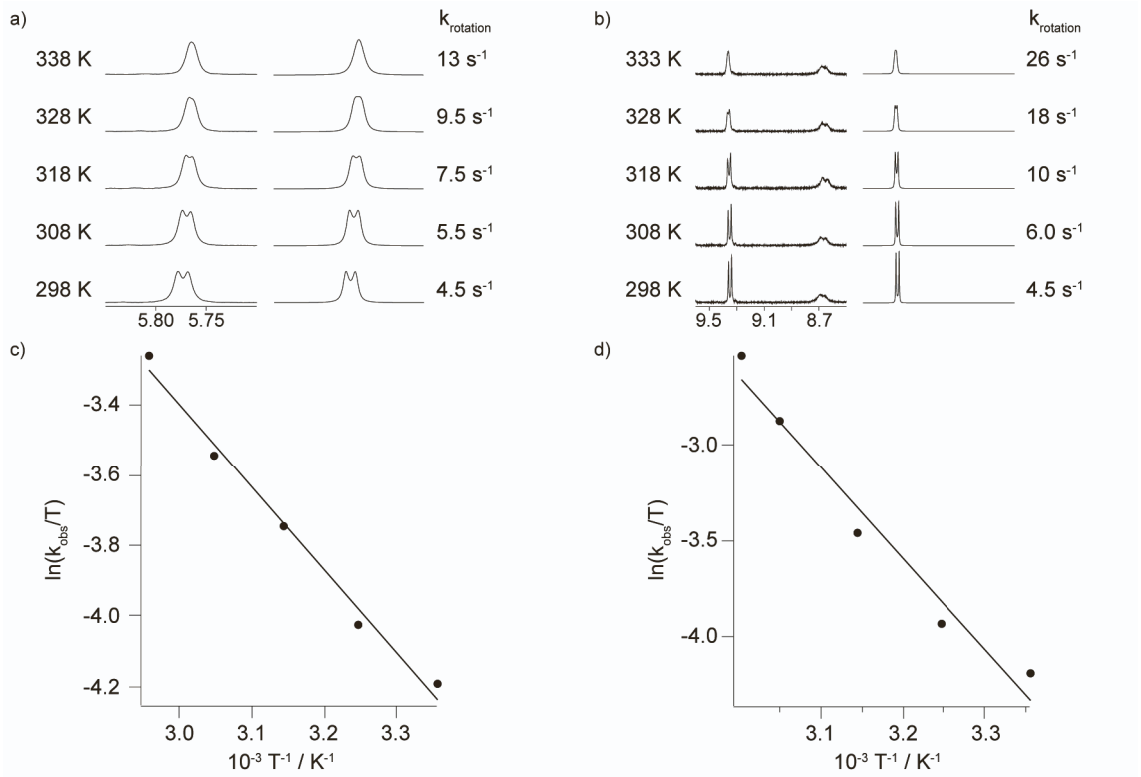

Figure S16. Partial ^{1}H-NMR (500 MHz, $CDCl_3$) spectra of $\mathbf{1}^{2+}\cdot 2PF_6^-$ (a) and $\mathbf{2}^{2+}\cdot 2\ PF_6^-$ (b) at different temperatures (left) and corresponding simulated NMR spectra of exchanging protons $H_4^{c/E}$ and $H_4^{c/Z}$ and $H_5^{c/E}$ and $H_5^{c/Z}$ respectively (right). Corresponding exchange rate constants ($k_{rotation}$) are reported on the right column (for assignment see text). c) Eyring plot for the rotation process in $\mathbf{1}^{2+}\cdot 2PF_6^-$. d) Eyring plot of the sole amide rotation process in $\mathbf{2}^{2+}\cdot 2PF_6^-$.

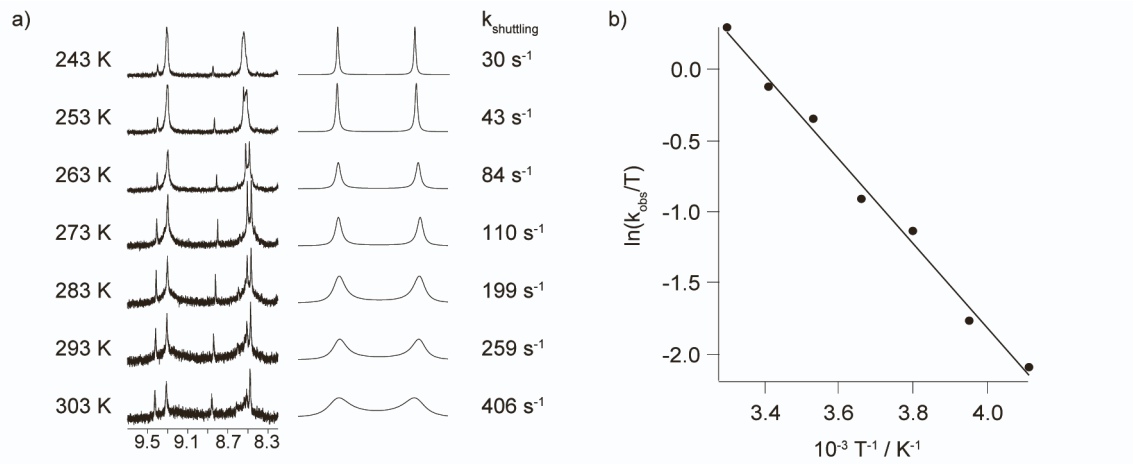

Figure S17. Partial ^{1}H-NMR (500 MHz, $CDCl_3$) spectra (a) of **1b**$^{2+}$·2PF_6^- at different temperatures (left) and corresponding simulated NMR spectra of the exchanging protons H_5^u and H_5^c (right). Corresponding exchange rate constants ($k_{shuttling}$) are reported on the right column (for assignment see text). b) Eyring plot for the shuttling process in **1b**$^{2+}$·2PF_6^-.

3.6.3. Comprehensive table of the activation parameters

Table S4. Activation parameters for the isomerization of **1**$^{2+}$·2PF_6^-, **1a**$^{2+}$·2PF_6^-, **1b**$^{2+}$·2PF_6^-, **2**$^{2+}$·2PF_6^-, and **2a**$^{2+}$·2PF_6^- in DMSO-d_6 and in $CDCl_3$.

	DMSO-d_6			$CDCl_3$		
	$\Delta G^{\ddagger}$ [(a)] (kJ mol^{-1})	$\Delta H^{\ddagger}$ (kJ mol^{-1})	$\Delta S^{\ddagger}$ (J mol^{-1} K^{-1})	$\Delta G^{\ddagger}$ [(a)] (kJ mol^{-1})	$\Delta H^{\ddagger}$ (kJ mol^{-1})	$\Delta S^{\ddagger}$ (J mol^{-1} K^{-1})
1^{2+}·2PF_6^-						
(rotation)	73.8 ± 9.0	30.3 ± 3.3	–145.7 ± 8.5	69.4 ± 9.2	19.7 ± 2.4	–167 ± 9
(shuttling)	85.2 ± 8.2	46.0 ± 3.3	–131.3 ± 8.5	[(b)]	[(b)]	[(b)]
1a^{2+}·2PF_6^-	79.6 ± 8.3	54.1 ± 1.1	–85.7 ± 8.8	[(c)]	[(c)]	[(c)]
1b^{2+}·2PF_6^-	52 ± 10[(d)]	24.8 ± 3.5[(d)]	–91 ± 12[(d)]	58.6 ± 8.9	24.6 ± 2.9	–114 ± 11
2^{2+}·2PF_6^-	72 ± 17	58.3 ± 4.1	–46 ± 13	70 ± 15	39.6 ± 0.4	–101 ± 11
2a^{2+}·2PF_6^-	72 ± 20	54.4 ± 4.1	–59 ± 13	[(c)]	[(c)]	[(c)]

The error on the activation parameters is a 95% confidence interval. (a) Determined at 298 K; (b) too slow to be determined; (c) value not determined; (d) estimated from residual line broadening after coalescence.

Activation parameters determined for **1a**$^{2+}$ and **2a**$^{2+}$ are in line with data reported for similar amides,[9] confirming that the axle substituents do not influence the amide rotation dynamic. The free enthalpy of activation at 298 K for **2a**$^{2+}$ (72 kJ/mol) is lower than that of **1a**$^{2+}$ (79.6 kJ/mol) due to the inductive effect of the methyl group directly connected to the carbonyl group.[10] For **1**$^{2+}$ and **2**$^{2+}$ the free enthalpy of activation for rotation about the CN-CO bond is lower in chloroform than in DMSO, in line with previous observations in the literature.[11]

The activation parameters for **1b**$^{2+}$ in $CDCl_3$ are in line with those reported previously in CD_2Cl_2.[1]

3.7. Uncertainty of the activation parameters

The variance of the activation parameters extracted from the Eyring plots was evaluated according to equations 3 and 4 derived by Girolami.[12] The uncertainty on the calculated $\Delta G^{\ddagger}$ was estimated by applying standard error propagation to the Gibbs function (equation 5). The errors in the exchange rate constants (σk) of ca. 5% were estimated on the basis of a subjective judgment of the sensitivities of the fits to changes in the rate constants. The estimated error in the temperature (σT) measurements was 0.1 K. The errors reported in table S4 are 95% confidence intervals calculated as double of the standard deviation.

$$\sigma(\Delta H^{\ddagger})^2 = \left(\frac{\mathrm{R}T_{max}T_{min}}{\Delta T}\right)^2 \left\{\left(\frac{\sigma T}{T}\right)^2 \left[\left(1 + T_{min}\frac{\Delta L}{\Delta T}\right)^2 + \left(1 + T_{max}\frac{\Delta L}{\Delta T}\right)^2\right] + 2\left(\frac{\sigma k}{k}\right)^2\right\}$$

Equation 3. Variance on $\Delta H^{\ddagger}$. R: universal gas constant; $\Delta L = \ln(k_{max}/T_{max}) - \ln(k_{min}/T_{min})$; $\Delta T = T_{max} - T_{min}$.

$$\sigma(\Delta S^{\ddagger})^2 = \left(\frac{\mathrm{R}}{\Delta T}\right)^2 \left\{\left(\frac{\sigma T}{T}\right)^2 \left[{T_{max}}^2\left(1 + T_{min}\frac{\Delta L}{\Delta T}\right)^2 + {T_{min}}^2\left(1 + T_{max}\frac{\Delta L}{\Delta T}\right)^2\right] + \left(\frac{\sigma k}{k}\right)^2\left({T_{max}}^2 - {T_{min}}^2\right)\right\}$$

Equation 4. Variance on $\Delta S^{\ddagger}$. R: universal gas constant; $\Delta L = \ln(k_{max}/T_{max}) - \ln(k_{min}/T_{min})$; $\Delta T = T_{max} - T_{min}$.

$$\sigma(\Delta G^{\ddagger}) = \Delta G^{\ddagger}\sqrt{\left(\frac{\sigma \Delta H^{\ddagger}}{\Delta H^{\ddagger}}\right)^2 + \left(\frac{\sigma T}{T}\right)^2 + \left(\frac{\sigma \Delta S^{\ddagger}}{\Delta S^{\ddagger}}\right)^2}$$

Equation 5. Standard deviation on $\Delta G^{\ddagger}$.

4. NMR spectra

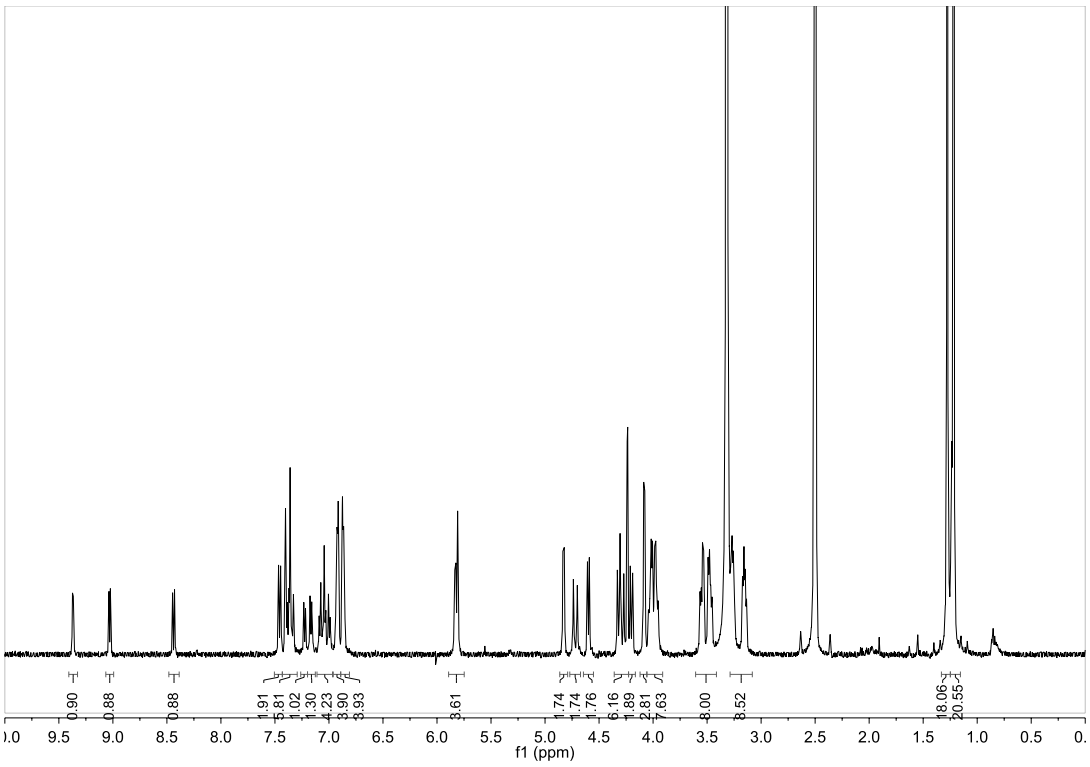

Figure S18. ^{1}H NMR spectrum of $\mathbf{1}^{2+}\cdot 2PF_6^-$ (500 MHz, DMSO-d_6, 298 K).

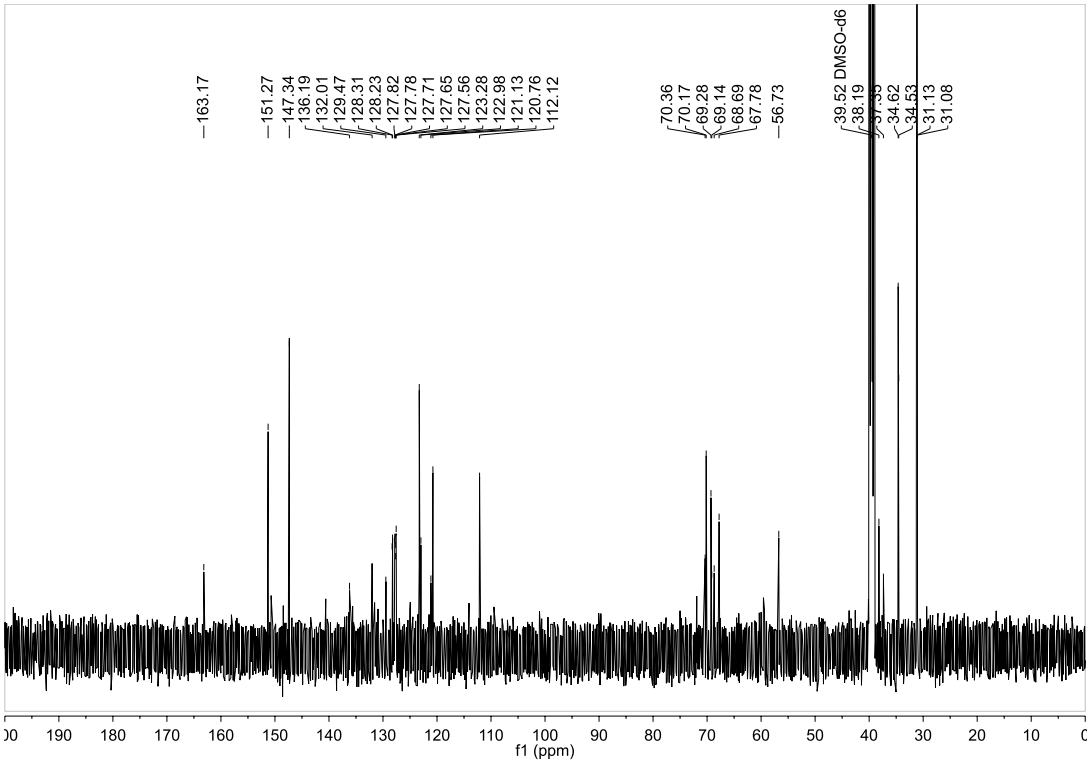

Figure S19. ^{13}C NMR spectrum of $\mathbf{1}^{2+}\cdot 2PF_6^-$ (125 MHz, DMSO-d_6, 298 K).

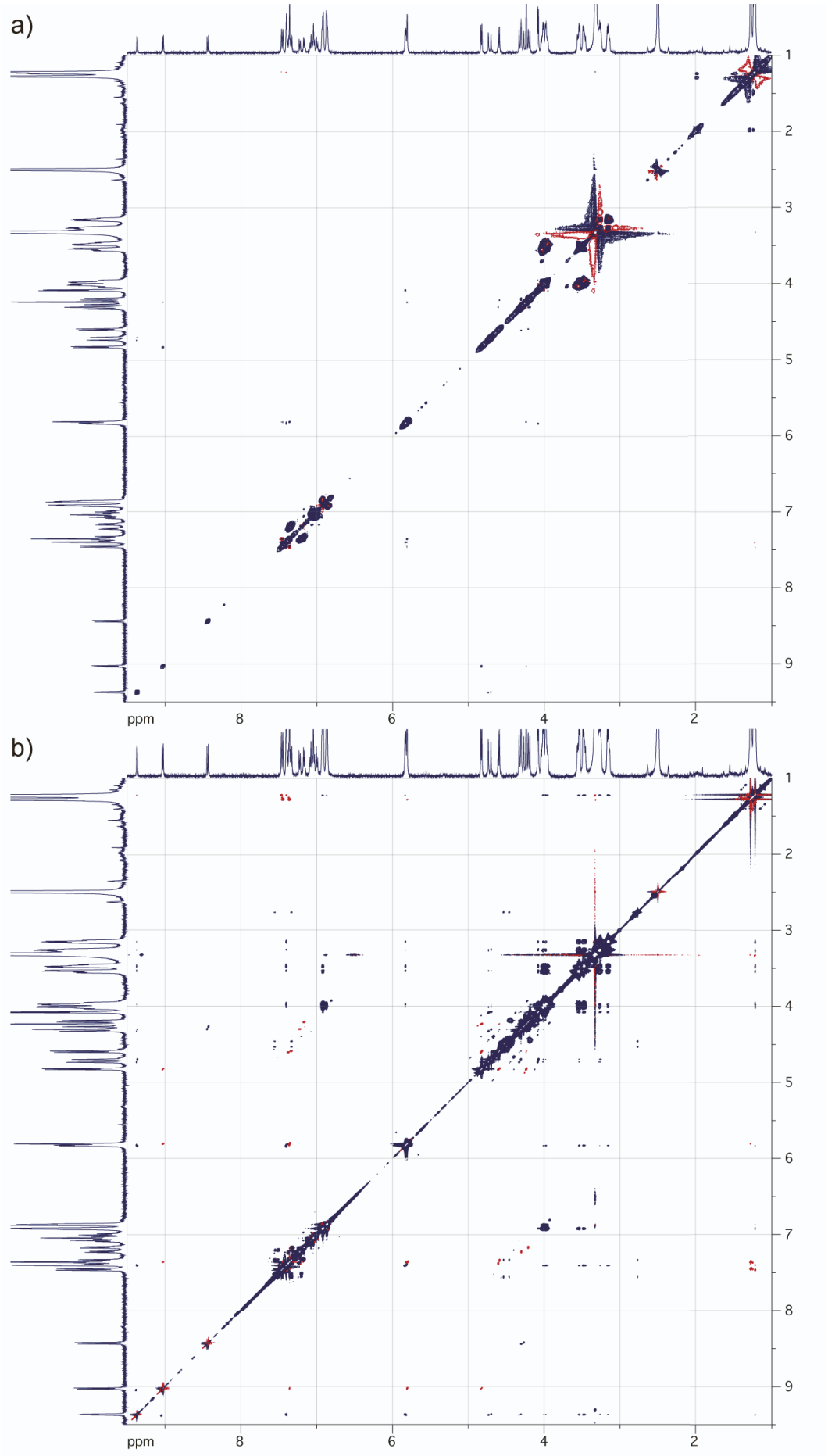

Figure S20. Bidimensional NMR spectra of $\mathbf{1}^{2+}\cdot 2PF_6^-$. a) TOCSY spectrum (500 MHz, DMSO-d_6, 298 K, spinlock 80 ms). b) NOESY spectrum (500 MHz, DMSO-d_6, 298 K, t_{mix} = 0.4 s).

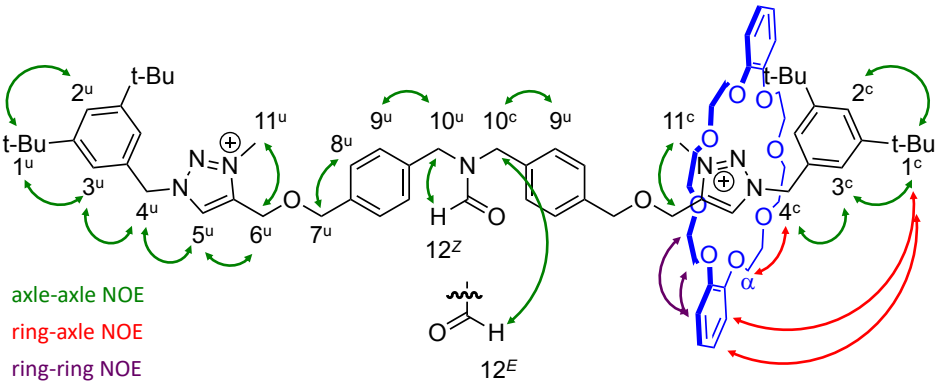

Figure S21. NOE mapping of ***E*-1**$^{2+}$ and ***Z*-1**$^{2+}$.

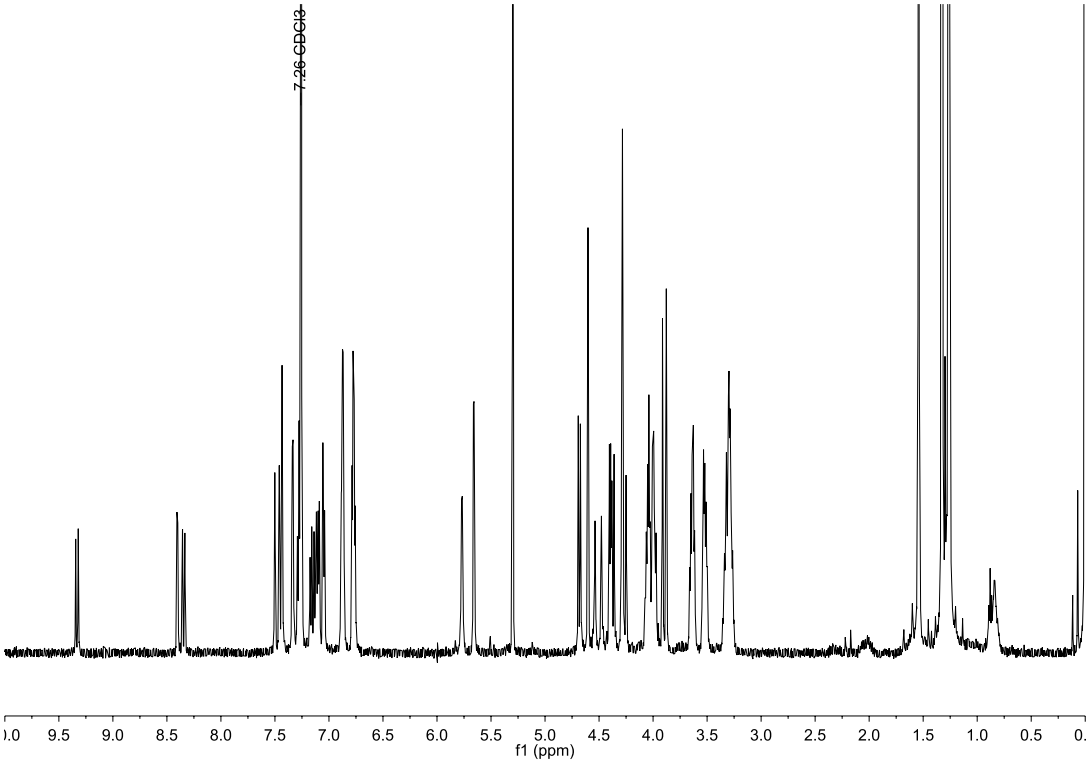

Figure S22. ^{1}H NMR spectrum of **1**$^{2+}\cdot 2PF_6^-$ (500 MHz, $CDCl_3$, 298 K).

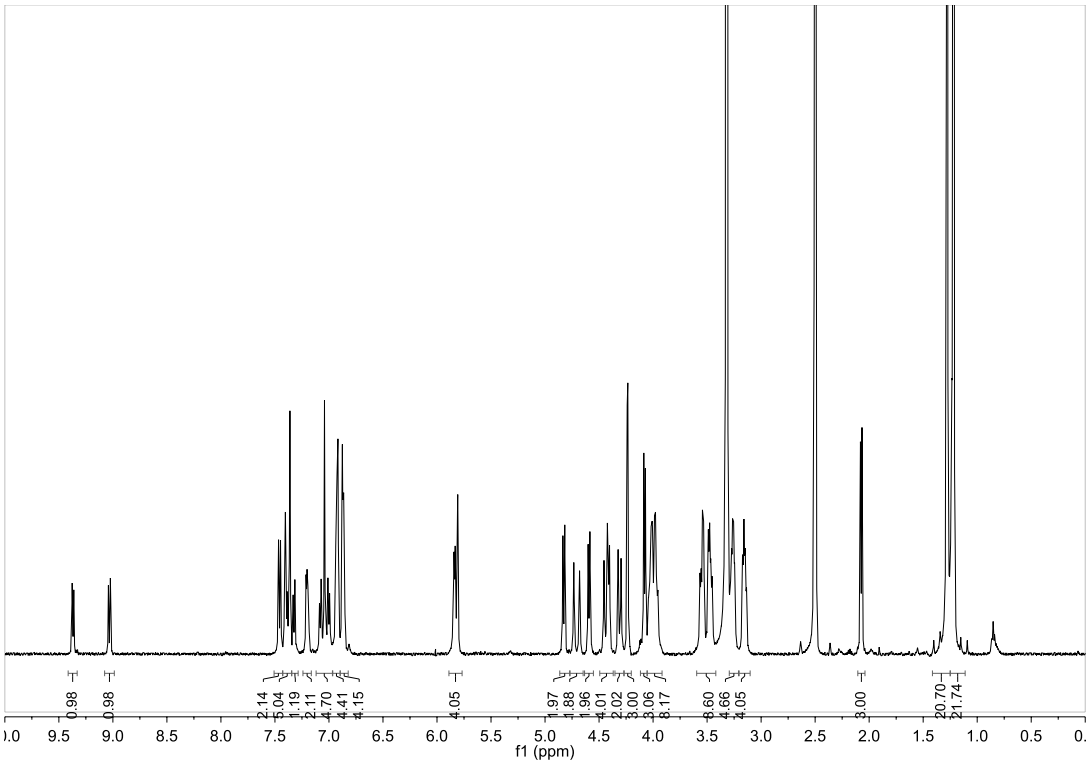

Figure S23. ^{1}H NMR spectrum of $\mathbf{2}^{2+}\cdot 2PF_6^-$ (500 MHz, DMSO-d_6, 298 K).

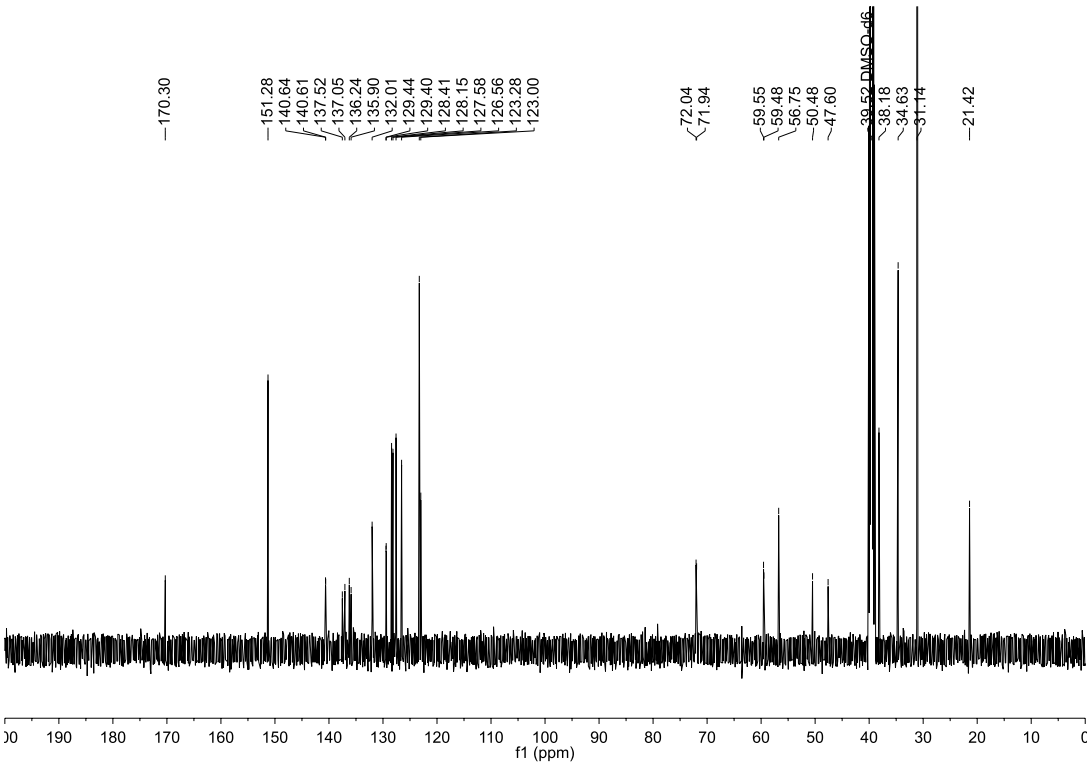

Figure S24. ^{13}C NMR spectrum of $\mathbf{2}^{2+}\cdot 2PF_6^-$ (125 MHz, DMSO-d_6, 298 K).

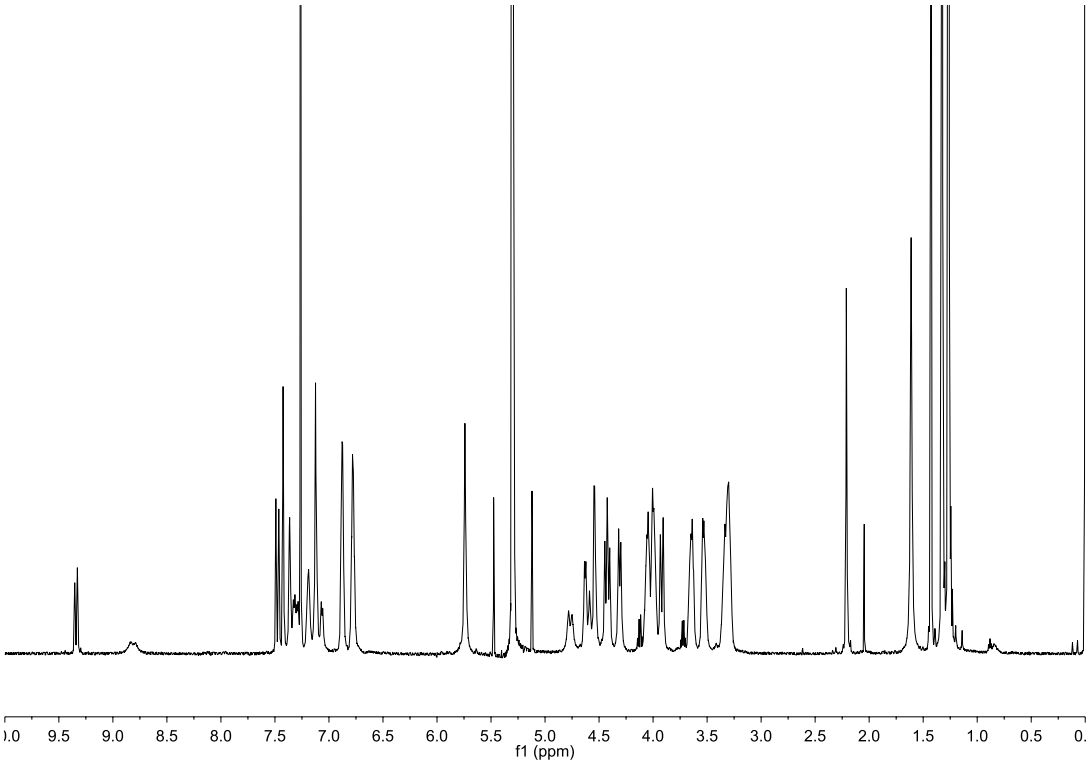

Figure S25. ^{1}H NMR spectrum of $\mathbf{2}^{2+}\cdot 2PF_6^-$ (500 MHz, $CDCl_3$, 298 K).

The broadening of the resonances observed for $\mathbf{2}^{2+}\cdot 2PF_6^-$ is due to a faster interconversion in the ^{1}H NMR timescale between the two stereoisomers in $CDCl_3$ compared to DMSO-d_6.[10,11]

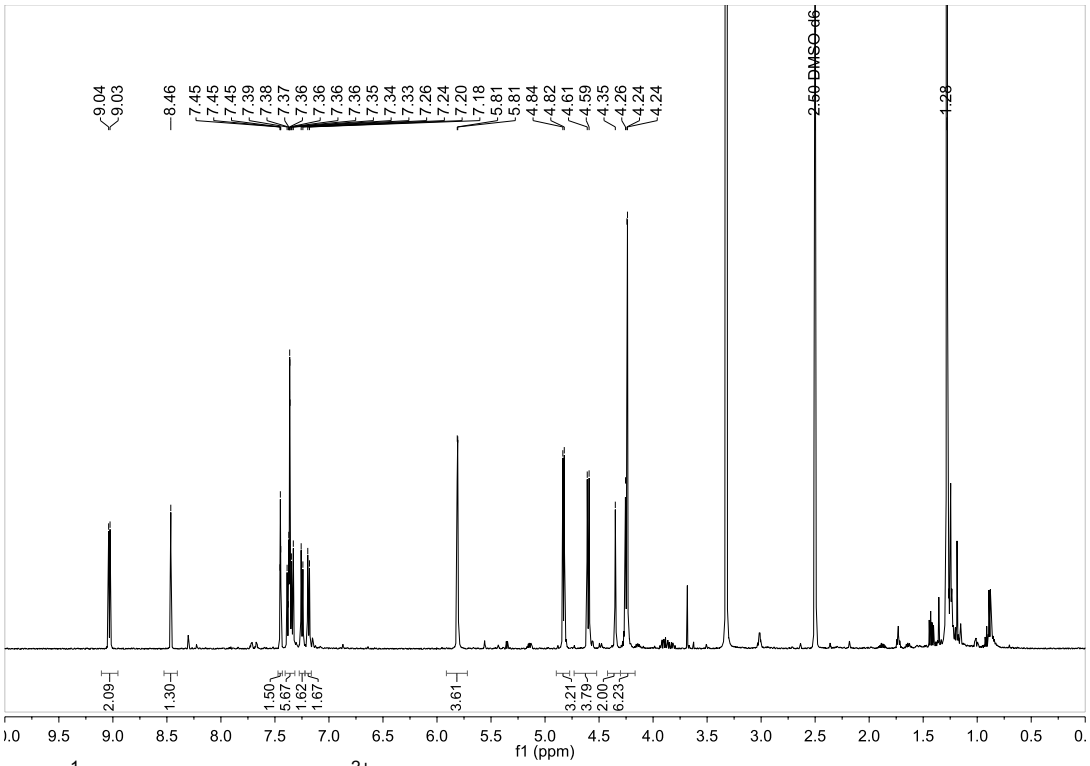

Figure S26. ^{1}H NMR spectrum of **1a**$^{2+}$·2PF_6^- (500 MHz, DMSO-d_6, 298 K).

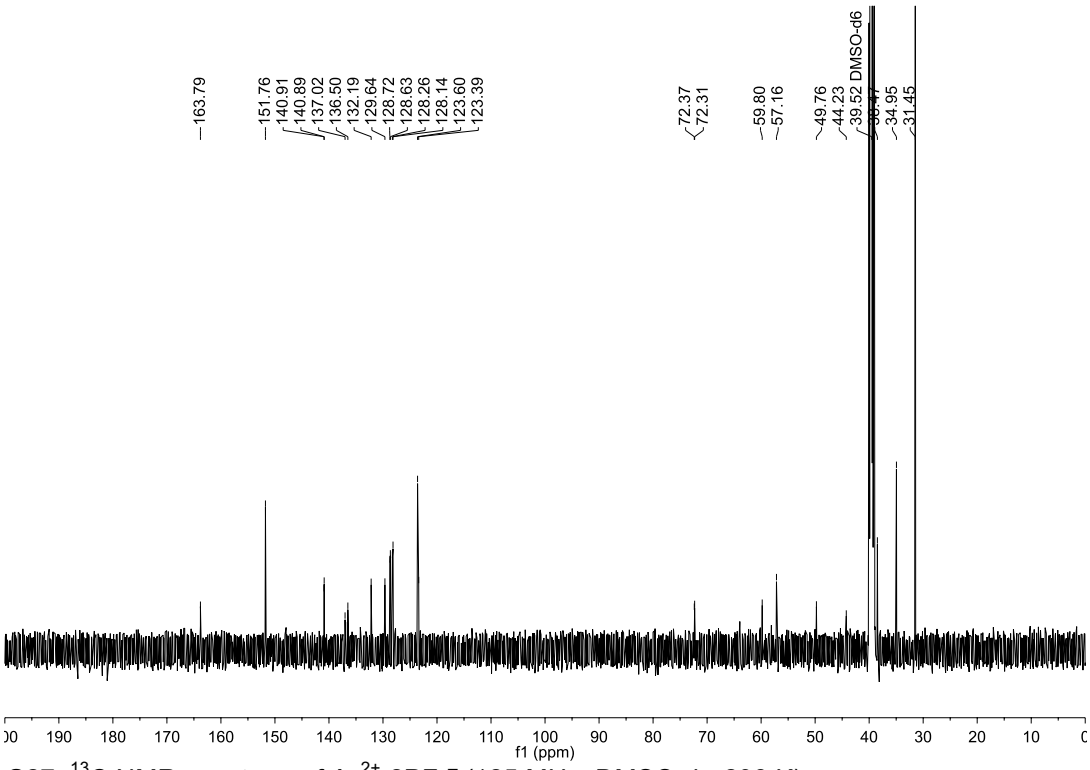

Figure S27. ^{13}C NMR spectrum of **1a**$^{2+}$·2PF_6^- (125 MHz, DMSO-d_6, 298 K).

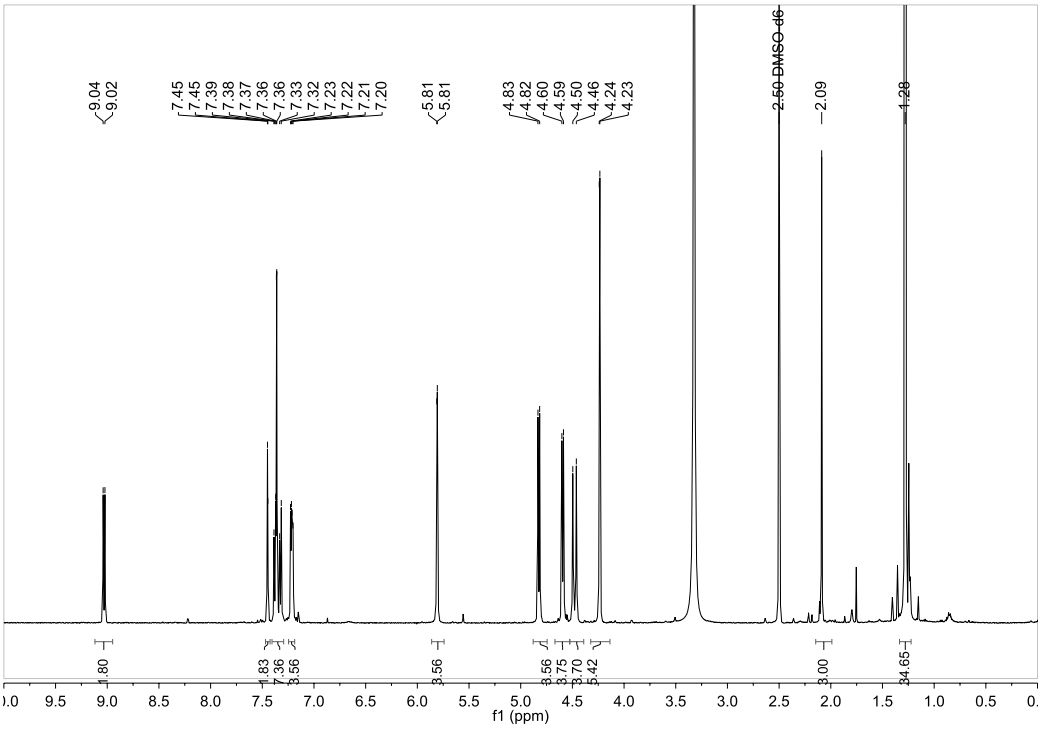

Figure S28. ^{1}H NMR spectrum of **2a**$^{2+}$·2PF_6^- (500 MHz, DMSO-d_6, 298 K).

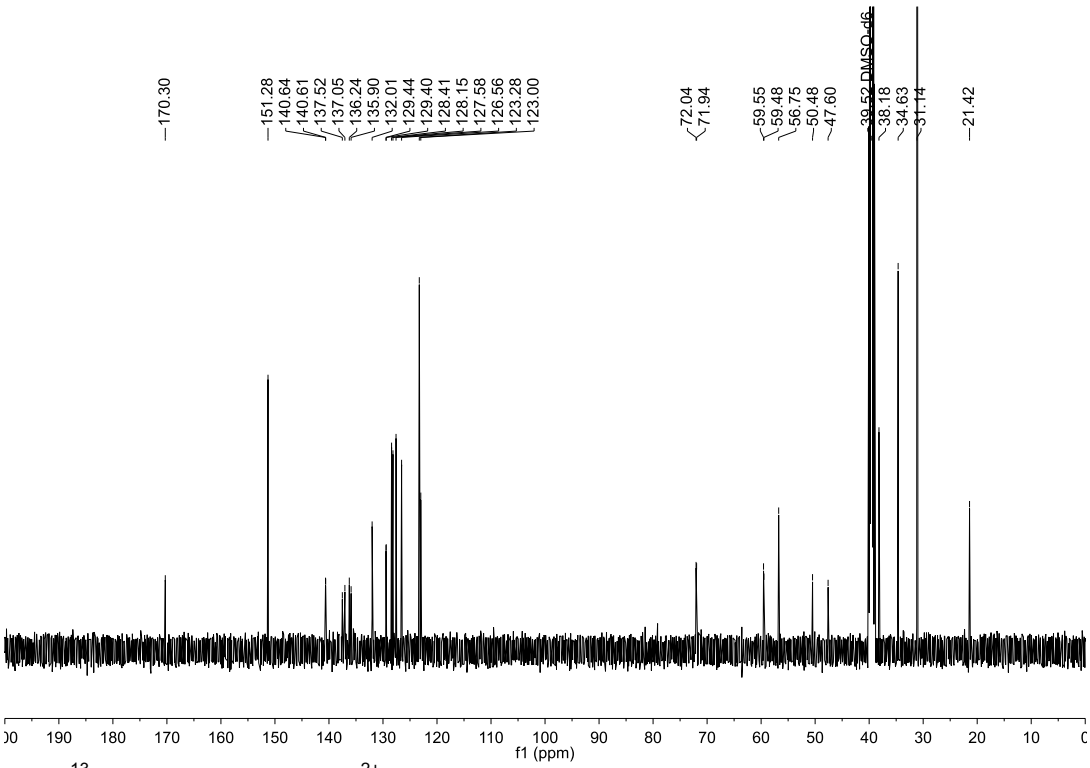

Figure S29. ^{13}C NMR spectrum of **2a**$^{2+}$·2PF_6^- (125 MHz, DMSO-d_6, 298 K).

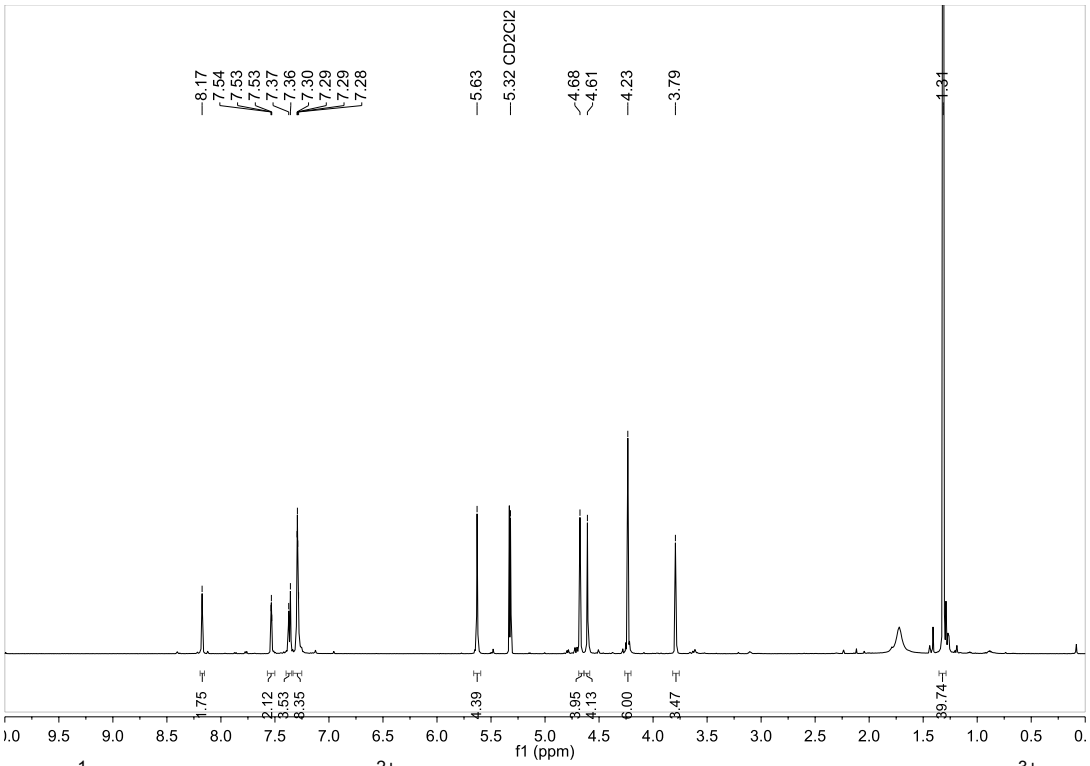

Figure S30. ^{1}H NMR spectrum of **S6**$^{2+}$·2PF_6^- (500 MHz, CD_2Cl_2, 298 K). Compound **S6**H^{3+}·3PF_6^- was deprotonated *in situ* with polymer-bound BEMP.

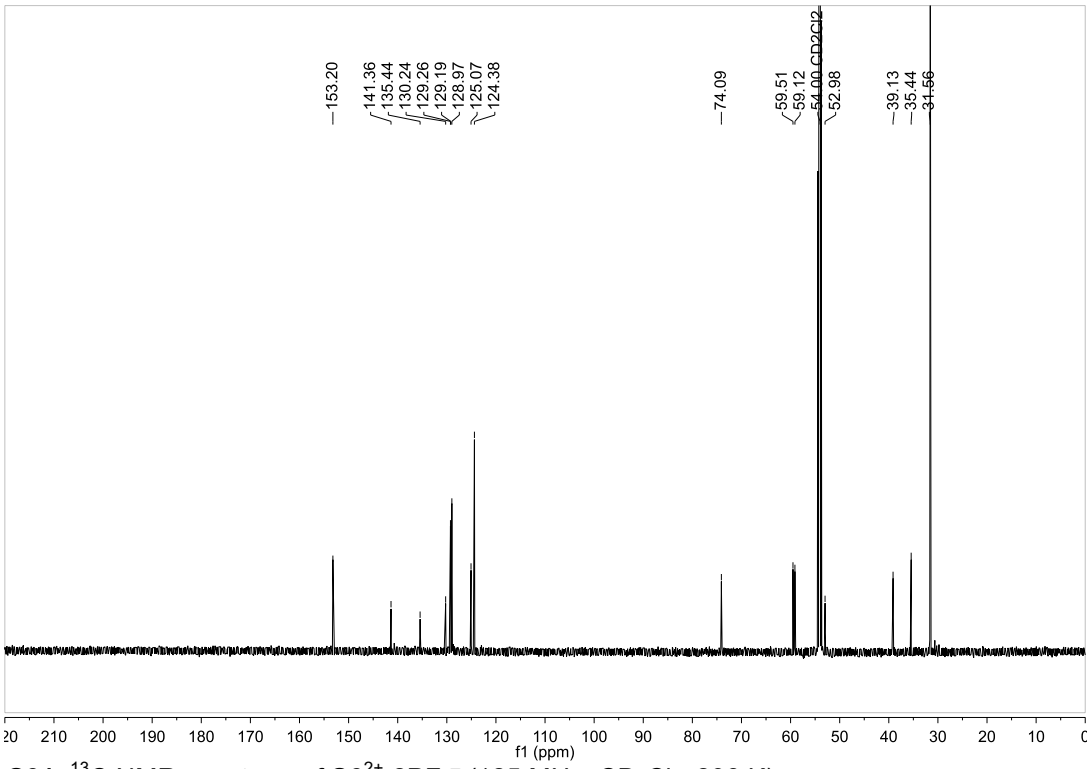

Figure S31. ^{13}C NMR spectrum of **S6**$^{2+}$·2PF_6^- (125 MHz, CD_2Cl_2, 298 K).

5. References

[1] Corra, S., de Vet, C., Groppi, J., La Rosa, M., Silvi, S., Baroncini, M., and Credi A. (2019). Chemical on/Off Switching of Mechanically Planar Chirality and Chiral Anion Recognition in a [2]Rotaxane Molecular Shuttle. J. Am. Chem. Soc. *141*, 9129–9133.

[2] Ragazzon, G., Credi, A., and Colasson, B. (2017). Thermodynamic Insights on a Bistable Acid–Base Switchable Molecular Shuttle with Strongly Shifted Co-conformational Equilibria. Chem. Eur. J. *23*, 2149–2156.

[3] Alvarez-Pérez, M., Goldup, S. M., Leigh, D. A., and Slawin, A. M. Z. (2008). A Chemically-Driven Molecular Information Ratchet. J. Am. Chem. Soc. *130*, 1836–1838.

[4] Hirota, M., Sakaibara, K., Suezawa, H., Yuzuri, T., Ankai, E., and Nishio, M. (2000). Intramolecular CH-π interaction. Substituent effect as a probe for hydrogen bond-like character. J. Phys. Org. Chem. *13*, 620–623.

[5] Williams, T. J., Kershaw, A. D., Li, V., and Wu, X. (2011). An Inversion Recovery NMR Kinetics Experiment. J. Chem. Educ. *88*, 665–669.

[6] Bain, A. D., and Cramer, J. A. (1996). Slow Chemical Exchange in an Eight-Coordinated Bicentered Ruthenium Complex Studied by One-Dimensional Methods. Data Fitting and Error Analysis. J. Magn. Reson. *118A*, 21–27.

[7] Since magnetization in the tens of thousands can give numerical problems, as noted by Bain *et. al.*,[6] each series of magnetization values was normalized to its final value in order to provide a set of data in the 10^0 order of magnitude. Such a manipulation does not affect the fitting results (see ref. 6 and CIFIT user's manual).

[8] Waelès, P., Clavel, C., Fournel-Marotte, K., and Coutrot, F. (2015). Synthesis of triazolium-based mono- and trisbranched [1]rotaxanes using a molecular transporter of dibenzo-24-crown-8. Chem. Sci. *6*, 4828–4836.

[9] Stewart, W. E., and Siddall T. H. (1970). Nuclear Magnetic Resonance Studies of Amides. Chem. Rev. *70*, 517–551.

[10] Drakenberg, T., Dahlqvist, K.-I., and Forsén, S. (1972). The Barrier to Internal Rotation in Amides. IV. N,N-Dimethylamides; Substituent and Solvent Effects J. Phys. Chem. *76*, 2178–2183.

[11] Wiberg, K. B., Rablen, P. R., Rush, D. J., and Keith, T. A. (1995). Amides. 3. Experimental and Theoretical Studies of the Effect of the Medium on the Rotational Barriers for N,N-Dimethylformamide and N,N-Dimethylacetamide. J. Am. Chem. Soc. *117*, 4261–4270.

[12] Morse, P. M., Spencer, M. D., Wilson, S. R., and Girolami, G. S. (1994). A Static Agostic α-CH•••M Interaction Observable by NMR Spectroscopy: Synthesis of the Chromium(II) Alkyl $[Cr_2(CH_2SiMe_3)_6]^{2-}$ and Its Conversion to the Unusual "Windowpane" Bis(metallacycle) Complex $[Cr(\kappa^2\text{-}C,C'\text{-}CH_2SiMe_2CH_2)_2]^{2-}$. Organometallics *13*, 1646–1655.